Tectonophysics 868 (2023) 230084

Contents lists available at ScienceDirect

Tectonophysics

journal homepage: www.elsevier.com/locate/tecto

Characterization of carbonate veins in graywacke layers from the Humber zone (Quebec, Canada) and implications for strength recovery of damaged rocks by mineral precipitation

Shaocheng Ji [a,*], Tiantian Chen [b], Le Li [a,1], Chun'an Tang [c], Denis Marcotte [a]

[a] Département des Génies Civil, Géologique et des Mines, École Polytechnique de Montréal, Montréal, Québec H3C 3A7, Canada
[b] School of Resources and Civil Engineering, Northeastern University, Shenyang 110819, China
[c] State Key Laboratory of Coastal and Offshore Engineering, Dalian University of Technology, Dalian 116024, China

ARTICLE INFO

Keywords:
Rock fracture mechanics
Sedimentary rocks
Veins
Joints
Strength recovery fracture healing/sealing

ABSTRACT

The Humber zone's Paleozoic sedimentary rocks, located on the rocky beaches of the Saint-Lawrence River in Quebec, Canada, exhibit interlayered calcareous greywacke beds and ductile shale. Fractures within these layers are characterized by either carbonate veins or barren joints, which are parallel arrays of planar fractures aligned in similar orientations. Fracture initiation occurred at either lithological interfaces or within brittle layers. The thickness of carbonate veins increases linearly with either bed thickness or layer-parallel extension strain, and carbonate precipitation occurred either simultaneously or ephemerally after the fracture opened. For a given bed thickness, veins are more closely and regularly spaced than joints, a feature that was successfully modeled using 2D finite element modeling. Both veins and joints follow a power-law relation between fracture spacing (s) and bed thickness (t), yielding a Weibull modulus of ~2.5, a tensile strength of ~9 MPa for the greywacke, and a shear flow strength of ~1 MPa for the shale at the time of fracture formation. The different s-t relationships observed between joints and veins indicate that carbonate cementation results in 60% strength recovery for greywacke layers in the study area. This approach provides a new constraint on the degree of rock strength recovery due to mineral precipitation into opening fractures under natural conditions. The cementation-induced strength recovery inhibits stress axis permutation, and consequently, suppresses the formation of orthogonal veins.

1. Introduction

The Earth sciences face a difficult problem in quantitatively estimating the degree of rock strength recovery resulting from mineral cements precipitated into opening fractures in natural rocks, using field-collected data. Tectonic deformation causes brittle fractures in rocks in the upper part of the crust, reducing their mechanical strengths and stability. The healing or sealing of these fractures can lead to strength recovery but also reduced permeability (e.g., Fagereng, 2011; Virgo et al., 2014), affecting mechanical properties, seismic velocities, and the flow of groundwater, geothermal water, and hydrocarbons (Morrow et al., 2001; Olivier et al., 2015; Aben et al., 2017). In the petroleum industry, hydraulic fractures are created to increase the permeability of reservoir rocks and thus the productivity of oil and gas (Bennion et al., 1996; Wang et al., 2014). However, if these fractures become partially or entirely sealed by mineral precipitation, the permeability of fractured reservoirs may be reduced (e.g., Gudmundsson and Brenner, 2001). Injecting $CaCO_3$ saturated solution to seal hydraulic fractures after extracting gas or oil from the reservoirs may be an effective way to protect the environment and mitigate seismic activity (Jones and Detwiler, 2016; Tobler et al., 2018). In particular, cementation-induced strength recovery and buildup of pore fluid pressure in fault zones can cause earthquakes to recur. Both theoretical and practical importance has driven laboratory experiments (e.g., Lee and Morse, 1999; Tenthorey et al., 2003; Yasuhara et al., 2005; Tenthorey and Cox, 2006; Lee et al., 2015; Shang et al., 2016; Aben et al., 2017) and numerical simulations (Dobson et al., 2003; Vass et al., 2014; Virgo et al., 2014; Hooker and Katz, 2015) to study the strength recovery of damaged

* Corresponding author.
E-mail address: sji@polymtl.ca (S. Ji).
[1] Present address: College of Earth Sciences, Chengdu University of Technology, Chengdu, 610059, China.

https://doi.org/10.1016/j.tecto.2023.230084
Received 18 February 2023; Received in revised form 26 September 2023; Accepted 27 September 2023
Available online 31 October 2023

rocks, but field observation-based quantified assessments are still limited. Therefore, understanding the relationship between mineral precipitation and strength recovery from direct field observations is essential.

The geological definition of joints and veins is that joints are barren, or not mineralized, fractures or fissures, while veins are mineral-filled or cemented fractures (Peacock, 2004). Both joints and veins are sets of planar and parallel fractures with little or no shear displacement, and they are aligned perpendicularly to the minimum principal stress at the time of their formation. Hooker and Katz (2015) pioneered to report that the ratios of fracture spacings (s) to bed thicknesses (t) are significantly smaller for veins than for joints, based on a literature review of data from multiple lithologies with varying stresses, strains, structures, and tectonic histories (Table 1 of Hooker and Katz, 2015). However, to verify the universality of their findings, it is necessary to obtain high-quality data from the same lithology deformed under the same conditions.

Veins are ancient fractures that have been filled with minerals as a result of mineral precipitation and were formed at great depths before being exposed on the Earth's surface. The study of vein geometrical patterns can provide insights into the processes and mechanisms involved in their formation, as well as provide valuable information on the degree of rock strength recovery by mineral cements that have precipitated into open fractures under natural deformation conditions. In this study, we present our new data on the geometrical features of carbonate veins in calcareous greywacke beds interlayered with shale from the rocky beach of the southern shore of the Saint-Lawrence River in Gaspésie, Quebec, Canada (Fig. 1). We demonstrate how the field-collected data, in conjunction with two-dimensional (2D) finite element modeling, can be utilized to enhance our understanding of the recovery of damaged rocks' strength through carbonate precipitation.

2. Geological setting

The Humber Zone of the Quebec Appalachians in Canada (Fig. 1) comprises folded sedimentary rocks, including the Saint-Roch Formation (Early-to-Middle Cambrian), the Tourelle and Rivière Ouelle Formations (Early Ordovician), and the Cloridorme Formation (Middle Ordovician) (Strong and Walker, 1981; Ji and Saruwatari, 1998; Ji and Li, 2020). These rock formations are arranged as northwest-verging nappes, separated by southeast-dipping thrust faults. They were deformed during the Middle to Late Ordovician Taconian orogeny and the Middle Devonian Acadian orogeny (St-Julien, 1967; St-Julien and Hubert, 1975; Cousineau, 1998; Malo, 2004), which resulted from the collision of the Laurentia continental margin with a volcanic island arc above a southeast-dipping subduction slab at that time (Williams, 1995; Lavoie et al., 2003; Pincivy, 2003; Malhame and Hesse, 2015). The Logan's line, a major thrust fault, delineates the northwestern boundary of the allochthonous Humber zone (Williams, 1995), while the para-autochthonous domain is situated to the northwest of the Logan's line (St-Julien, 1967; Pinet et al., 2014).

The graywacke beds exposed in the region of Ste-Anne-des-Monts, which belong to the Early Ordovician Tourelle Formation, consist of quartz (~45%), feldspar (~8%), calcite (~17%), accessory minerals such as garnet, hypersthene and pyroxene (~1%), rock fragments (13%) and fine-grained (≤30 μm) matrix materials (~16%). The Tourelle Formation (up to 1000 m thick) has been folded and thrust by reverse faults (St-Julien and Hubert, 1975; Hiscott, 1978, 1980; Cousineau, 1998; Ji et al., 2021). According to Hiscott (1978), the detrital minerals, which constitutes the Tourelle Formation, came from not only the plutonic and metamorphic rocks of the Proterozoic Grenville Province but also the volcanic arc and ophiolite suite rocks. The latter were remained pieces of the oceanic plate consumed by subduction throughout the closing of the Iapetus Ocean (Williams, 1995). The graywacke beds exposed on the rocky beaches at Ste-Anne-des-Monts developed a dominant set of barren joints with an average attitude of (018°, 78°) (Fig. 2a).

The sedimentary strata that are exposed in the Rivière-à-Claude and Gros-Morne areas are part of the Early Ordovician Rivière Ouelle Formation. This formation is approximately 1000 m thick and is composed mainly of interbedded calcareous graywacke, limestone, and shale. Dolostone and fine-grained quartz arenite can also be found occasionally (Slivitzky et al., 1991). In the regions of Grande-Vallée and Petite-Vallée, the sedimentary strata are part of the Middle Ordovician Cloridorme Formation (Skipper and Middleton, 1975; Slivitzky et al., 1991). This formation comprises alternating layers of calcareous graywacke (38%), mudstone or shale (60%), and limestone (2%) and represents a succession of foreland sedimentary deposits with a total thickness of approximately 5700 m (Enos, 1969; Parkash, 1970; Skipper and Middleton, 1975; Slivitzky et al., 1991). The graywackes consist of detrital grains such as quartz, feldspars, mica, and rock fragments, as well as a fine-grained matrix of calcareous and argillaceous materials.

These formations, namely the Saint-Roch Formation, the Tourelle Formation, the Cloridorme Formation, and the Rivière Ouelle Formation, are Paleozoic-aged deformed sedimentary strata. They represent a series of north-directed tectonic nappes separated by south-dipping imbricate thrust faults within the Humber zone. These sediments were first deposited during the Cambrian to Middle and Late Ordovician on the passive margin slope, rise, and foredeep basin, and then thrust over the autochthonous Saint Lawrence Platform during the Taconian Orogeny (Late Ordovician, St-Julien et al., 1983; Lavoie, 2008; Lavoie et al., 2009; Hesse and Fong, 2014). Although the strata of these groups were folded and thrusted, they experienced little metamorphism, as indicated by the absence of penetrative schistosity in the argillaceous beds. The Appalachian Belt, which lies southeast of the Humber Zone (Fig. 1), consists of Upper Ordovician to Middle Devonian marine to continental sediments, and was considerably deformed and metamorphosed during the Middle Devonian Acadian Orogeny (St-Julien, 1967; Malo et al., 1995; Malo, 2004). Although the coastal exposures are of excellent quality, the region has been largely uninvestigated by structural geologists in terms of brittle fractures such as joints (Pinet et al., 2015; Ji et al., 2021) and veins.

3. Observations and measurements

Veins in calcareous graywacke beds were observed and measured along the coastal exposures in the Rivière-à-Claude, Gros-Morne, Grande-Vallée, and Petite-Vallée regions on the southern shore of the Saint-Lawrence River, Quebec, Canada (Fig. 1). The region's large tidal range provides continuous, fresh exposures of the Paleozoic sedimentary beds, enabling us to investigate the dependence of vein spacing (s) on bed thickness and the magnitude of layer-parallel extension required to form the veins in the graywacke beds. To examine the difference between joints and veins in terms of the s-t relationship, we also measured joints in the graywacke beds at Ste-Anne-des-Monts (Fig. 2b), where the joints have not been filled by carbonate precipitation to form veins. This exclusion of lithological effect makes it possible to compare the s-t relationship between joints and veins, as lithology is often an important factor influencing this relationship (e.g., Fischer et al., 1995; Ji et al., 2021).

3.1. General features

As illustrated in Fig. 3, the veins observed in the calcareous graywacke beds are planar, parallel fractures that have opened to allow minerals, mainly calcite and some quartz, to fill the voids. The differentiation between calcite and quartz was made by conducting HCl and scratch tests at the outcrops. The veins can be tracked for several meters, but the limited exposure continuity often restricts the observations. Unlike barren joint systems that typically comprise two sets of mutually perpendicular fractures (systematic and cross joints), creating an orthogonal network (Hancock, 1985; Gross, 1993; Bai et al., 2002; Li and Ji, 2021; Ji et al., 2023), the veins do not follow such a pattern in the

Table 1
Statistical data of vein spacing measured from calcareous greywacke beds in the Humber zone, Quebec, Canada.

No.	GPS coordinates		Location	t (cm)	Strain (%)	Vein spacing (cm)							t/s	s/t	C_v
	Latitude (°)	Longitude (°)				N	Mean	Median	St Dev	Mode	Skewness	Kurtsis			
44-Bed1	49.22150	65.88250	Rivière-à-Claude	54.5		8	34.9	37.0	9.6	N/A	−0.723	−0.609	1.47	0.68	0.275
44-Bed2	49.22150	65.88250	Rivière-à-Claude	28.0		6	26.7	24.9	8.2	N/A	0.965	0.243	1.12	0.89	0.306
44-Bed3	49.22150	65.88250	Rivière-à-Claude	32.8		35	33.4	28.0	22.0	38.0	0.466	−0.607	1.17	0.85	0.660
44-Bed4	49.22150	65.88250	Rivière-à-Claude	18.8		10	17.9	15.9	7.1	16.5	1.624	1.930	1.19	0.84	0.395
44-Bed5	49.22150	65.88250	Rivière-à-Claude	30.3		33	23.0	24.5	7.8	15.5	0.090	−1.111	1.24	0.81	0.340
53-Bed1	49.25325	65.54019	Gros-Morne	6.0		57	6.1	5.8	2.3	4.9	0.721	0.656	1.03	0.97	0.385
53-Bed2	49.25325	65.54019	Gros-Morne	4.9		9	8.0	8.8	3.2	N/A	−0.145	−1.559	0.56	1.80	0.400
53-Bed3	49.25325	65.54019	Gros-Morne	4.0		40	7.1	6.0	3.8	3.6	0.734	0.029	0.67	1.50	0.539
53-Bed4	49.25325	65.54019	Gros-Morne	5.1		13	13.8	13.5	4.7	N/A	0.006	0.030	0.38	2.65	0.344
54-Bed1	49.25328	65.52219	Gros-Morne	37.5		88	28.6	27.0	9.4	27.0	0.314	−0.303	1.39	0.72	0.330
54-Bed2	49.25328	65.52219	Gros-Morne	56.0		6	34.5	32.5	18.8	N/A	0.972	−0.158	1.72	0.58	0.544
57-Bed1	49.25342	65.54167	Gros-Morne	5.5	2.29	128	18.4	17.7	7.4	12.0	0.350	−0.138	0.31	3.21	0.403
57-Bed2	49.25342	65.54167	Gros-Morne	2.4	3.17	23	12.1	9.6	7.9	6.3	1.298	1.002	0.25	4.00	0.656
57-Bed3	49.25342	65.54167	Gros-Morne	8.0	4.79	95	15.0	13.6	7.0	15.7	0.607	−0.276	0.59	1.70	0.463
59-Bed1	49.22133	65.03589	Petite-Vallée	24.1	2.89	25	28.4	26.0	11.4	26.0	0.325	−0.591	0.93	1.08	0.401
59-Bed2	49.22133	65.03589	Petite-Vallée	21.0	2.37	42	20.3	20.7	8.3	17.1	0.638	2.298	1.01	0.99	0.408
60-Bed1	49.25403	65.53972	Gros-Morne	34.5	3.95	125	29.8	27.5	13.1	18.2	0.742	0.393	1.25	0.80	0.440
60-Bed2	49.25397	65.53928	Gros-Morne	13.2	3.84	81	22.3	19.5	12.7	11.1	0.761	0.123	0.68	1.47	0.572
62-Bed1	49.25458	65.53731	Gros-Morne	11.0	4.94	120	16.5	16.4	6.5	17.4	0.475	0.052	0.67	1.49	0.392
63-Bed1	49.25389	65.53972	Gros-Morne	8.0	3.78	175	13.1	12.6	4.4	12.2	0.737	0.754	0.63	1.58	0.335
64-Bed1	49.23072	65.13658	Grande Vallée	55.0	4.08	4	43.5	43.5	8.3	N/A	0.003	−5.979	1.27	0.79	0.192
64-Bed2	49.23072	65.13658	Grande Vallée	18.5	7.47	4	25.5	25.7	6.1	N/A	−0.068	−5.348	0.72	1.39	0.241
64-Bed3	49.23072	65.13658	Grande Vallée	27.0	3.03	13	34.8	37.5	14.2	N/A	0.286	−0.834	0.72	1.39	0.409
64-Bed4	49.23072	65.13658	Grande Vallée	283.0		21	121.6	120.0	42.6	121.0	0.509	−0.674	2.36	0.42	0.350
64-Bed5	49.23072	65.13658	Grande Vallée	17.5		11	22.5	19.5	6.9	18.0	0.890	−0.375	0.90	1.11	0.306
64-Bed6	49.23103	65.13686	Grande Vallée	102.0		26	79.3	72.5	27.6	78.0	0.735	−0.192	1.41	0.71	0.348
65-Bed1	49.22622	65.12658	Grande Vallée	42.5	5.27	22	50.8	53.8	17.9	57.0	0.030	−0.172	0.79	1.26	0.351
65-Bed2	49.22628	65.12661	Grande Vallée	13.8	3.29	31	28.1	25.6	14.0	27.2	1.240	1.772	0.54	1.85	0.496
65-Bed3	49.22639	65.12611	Grande Vallée	53.4	5.57	51	35.0	36.1	12.1	10.1	−0.076	−0.443	1.48	0.68	0.346
65-Bed4	49.22728	65.12544	Grande Vallée	32.8	5.03	36	29.2	27.3	11.0	26.5	0.026	−0.953	1.20	0.83	0.377
65-Bed5	49.22736	65.12569	Grande Vallée	18.6	2.72	19	22.0	19.0	10.2	N/A	0.866	−0.027	0.98	1.02	0.463
65-Bed6	49.22736	65.12567	Grande Vallée	49.5	8.47	11	38.3	37.0	12.2	29.0	1.184	0.965	1.34	0.75	0.319
65-bed7	49.22733	65.12572	Grande Vallée	11.6	1.40	7	17.3	16.4	4.4	N/A	0.460	−0.022	0.71	1.41	0.254
65-bed8	49.22753	65.12481	Grande Vallée	5.9		25	8.8	8.5	3.1	8.8	0.663	0.172	0.69	1.44	0.357
65-bed9	49.22767	65.12431	Grande Vallée	23.1	3.13	47	23.4	21.5	11.1	14.7	0.649	0.015	1.07	0.93	0.475
66-Bed1	49.22847	65.11389	Grande Vallée	20.4	2.18	58	27.0	27.6	11.5	35.4	0.269	−0.338	0.74	1.35	0.428

(*continued on next page*)

Table 1 (*continued*)

No.	GPS coordinates		Location	t (cm)	Strain (%)	Vein spacing (cm)							t/s	s/t	C_v
	Latitude (°)	Longitude (°)				N	Mean	Median	St Dev	Mode	Skewness	Kurtsis			
67-Bed1	49.22847	65.11347	Grande Vallée	7.8	3.67	45	14.2	12.3	6.3	9.0	0.620	−0.714	0.63	1.58	0.443
68 A	49.22858	65.11342	Grande Vallée	61.0	3.15	2	62.0	62.0	1.4	N/A			0.98	1.02	
68B	49.22858	65.11342	Grande Vallée	25.0	3.83	17	23.8	25.0	6.5	N/A	0.118	−0.692	1.00	1.00	0.273
69-Bed1	49.22811	65.11478	Grande Vallée	160.0	1.92	22	78.5	74.0	25.8	103.0	1.317	2.409	2.16	0.46	0.329
70-Bed1	49.22819	65.11467	Grande Vallée	15.7	1.62	59	29.1	26.6	12.1	18.9	0.429	−0.454	0.59	1.69	0.414

study area. This suggests that there are considerable differences in the formation mechanisms between joints and veins. The dilation veins are believed to have been formed by the precipitation of $CaCO_3$-rich aqueous solutions that were pumped or injected into low- or zero-pressure spaces created by the development of tensile fractures (Van Noten and Sintubin, 2010; Philipp, 2012; Gudmundsson, 2022; Späth et al., 2022). The reduction in pressure is considered the primary factor responsible for the oversaturation of the injected fluid with $CaCO_3$ and the subsequent crystallization of calcite.

Only <5% of the veins are found to cut across strata, indicating that the strata boundaries act as barriers for fracture propagation and fluid flow between beds with different mechanical properties (Cooke et al., 2006). The veins in the Gaspésie region are different from the non-stratabound Burren veins within metasediments documented by Gillespie et al. (2001) in Ireland and Van Noten and Sintubin (2010) in Germany. The Gaspésie veins within unmetamorphosed sedimentary rocks are stratabound and exhibit a strong dependence on scale, with vein spacing proportional to bed thickness (Fig. 3).

The veins are widespread along the coastal outcrops of the southern shore of the Saint-Lawrence River between Rivière-à-Claude and Petite-Vallée (Fig. 1). The outcrops generally trend eastward and dip moderately to subvertical to the south (Fig. 4a and Fig. S1), and have been folded with their northern limbs typically overturned, although overturned southern limbs are present in some areas (e.g., site 52). The fold hinges are usually subhorizontal, but can plunge up to 45° in some locations. The asymmetrical folds, which indicate a strong northward vergence, are interpreted as fault-propagation folds above blind, south-dipping, low-to-moderate angle thrusts that formed in response to north-south crustal shortening and thickening within the orogenic belt (Lynch, 1998; Lynch and Arsenault, 1997).

The veins in this area are commonly found perpendicular to the bedding plane and are preferentially aligned around a strike of 356° and a dip of 82° (Fig. 4b), approximately normal to the local hinges of north-verging, asymmetrical, overturned folds. One might assume that the veins are synchronous with folding and formed by local extension along the hinges of folds due to tectonic compression during the Taconic orogeny in the Appalachians. However, the veins are always normal or nearly perpendicular to the layers and have been rotated by folding and faulting (Fig. S1). By removing the effects of later folding and faulting, the reconstruction of the original orientations of the veins (Fig. 4c) suggests that the veins formed vertically by horizontal extension when the beds were flat-lying and were subsequently rotated with the beds by folding and faulting (Fig. S1d). No veins have been folded as they are limited in the competent beds, and the flexural folding was achieved by interbed slip. Therefore, the tensile fractures and carbonate precipitation predate the folding and faulting. A similar geochronological relationship between veins and folds was also documented in Cretaceous-Paleogene strata in Jordan (Hooker et al., 2017).

Horizontal veins are much less frequent than vertical ones. Along the boundaries of the graywacke bed with overlying and underlying shale layers at site 51 (GPS coordinates: 49.2282° N, 65.8595° W), bed-parallel veins were observed (Fig. S2). There is no indication that the horizontal veins result from the deflection of vertical veins (Gudmundsson, 2022). These bed-parallel veins are primarily made up of calcite fibers aligned parallel to the walls, suggesting that the crystals grew in spaces created by pull-apart along an uneven shear plane with micro-jogs. As depicted in Fig. S2, the graywacke layer includes closely spaced, layer-bound veins that are almost perpendicular to the bedding. The bed-parallel veins were created at the same time as the bed-normal veins, as demonstrated by cross-cutting relationships.

In graywacke beds displaying fossilized ripple marks in trough-and-crest formations on their top surfaces, a consistent observation has been made: bed-normal veins tend to be predominantly found at the troughs rather than the crests (Fig. S3). This observation suggests that the bed-parallel tensile stress, resulting from tectonic extension and/or overburden pressure, is specifically intensified at the troughs. As a consequence, the location of fractures (veins) may be influenced to some extent by the local shape and thickness of the layer, especially when these characteristics are non-uniform.

Three types of veins have been observed in the study area. (1) Lenticular-shaped veins with decreasing aperture towards the upper and lower boundaries of the bed, some of which do not appear to extend fully the layer boundaries on the observation surfaces (Fig. 5a). This type of veins suggests that the fractures originated from the interior of the competent layer and then propagated towards the upper and lower boundaries. (2) Veins with two quasi-parallel walls (as shown in Fig. 5b), indicating homogeneous displacement in the direction of extension. (3) Semi-lens-shaped veins, which typically have their greatest thicknesses at the boundaries (Fig. 5c), indicating that the fractures initiated from the interfaces and then propagated into the interior of the competent layer (Cooke et al., 2006).

Fig. 6 illustrates semi-lens-shaped veins that exhibit a tapering pattern directed towards the upper boundary of the layer at site 44 (GPS coordinates: 49.2215° N, 65.8825° W). Some veins observed on the surface of outcrops appear to terminate within the graywacke layers and fail to reach the upper boundaries with shale. It is noteworthy that there is no noticeable distinction in composition or microstructure between the upper and lower shale layers above and below the graywacke bed. These hydraulic fractures at this site are believed to have originated at the lower boundary and subsequently propagated primarily in an upward direction, facilitating the infiltration of $CaCO_3$-saturated fluids into the newly formed fractures. In the study area, veins originating from the lower boundaries of the beds are more prevalent compared to those originating from the upper boundaries.

The veins exhibit well-defined and distinct planar walls (Figs. 3, 5-6, S2, S3), and branching or finger-like patterns are uncommon (Fig. 7a), suggesting that the mechanism of fracture forking (Virgo et al., 2014) was not prevalent. Angular rock fragments are sometimes observed within the veins. Plume structures consisting of hackles are occasionally present along the preserved vein walls, suggesting rapid and dynamic crack propagation, rather than slow subcritical growth (Engelder and Fischer, 1996).

The veins exhibit no noticeable shear displacement (Figs. 3, 5-7), indicating that they opened in a direction perpendicular to their walls.

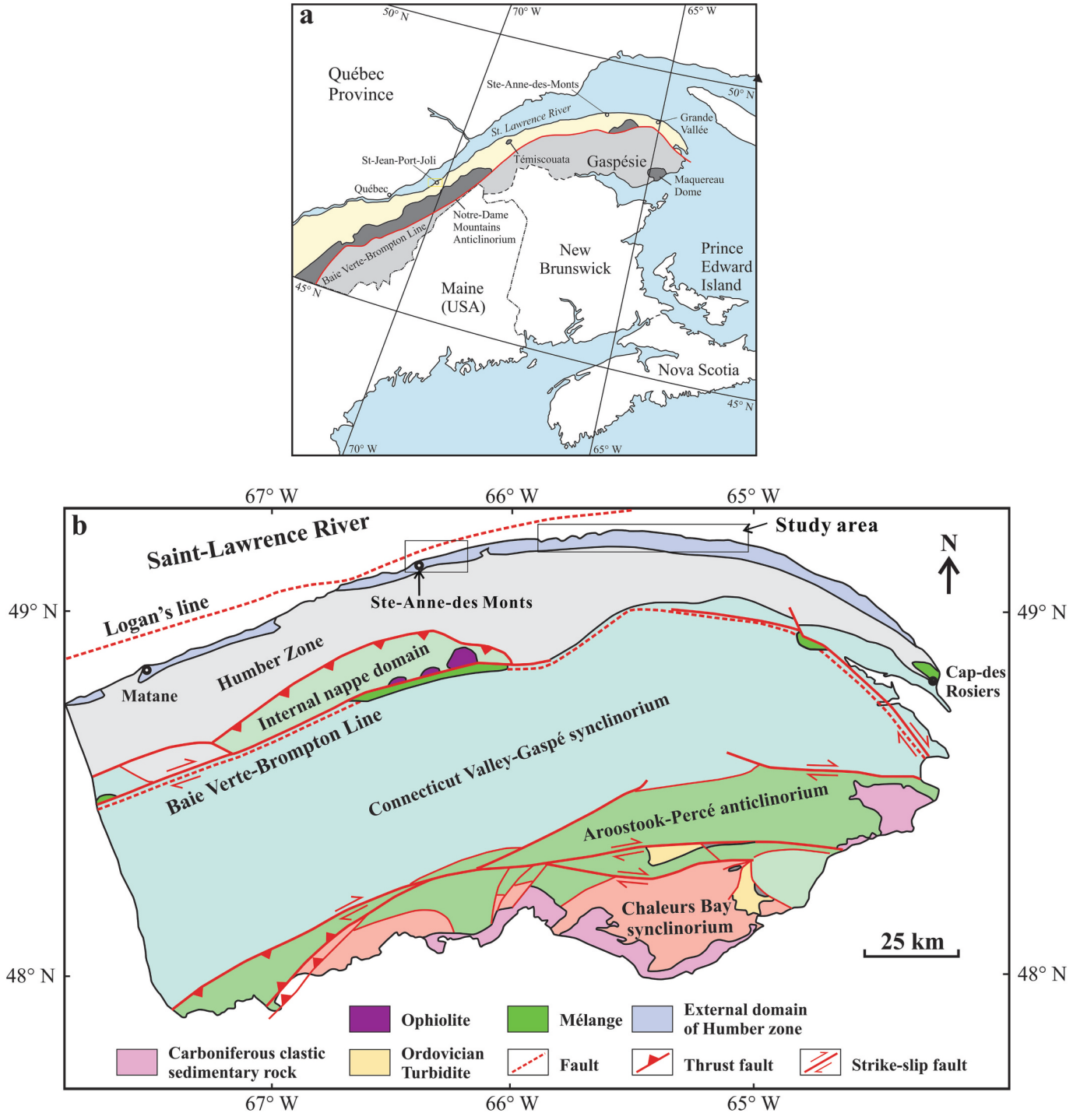

Fig. 1. Location and geological setting of the study area.

Short veins arranged in en echelon patterns occur in some minor fault zones. No sigmoidal veins have been observed, which suggests that there has been minimal cumulative shear deformation. Additionally, the veins are generally parallel to each other and are not deflected even when two adjacent veins cross (Figs. 3, 5-7). Previous studies (Olson and Pollard, 1989; Gillespie et al., 2001) have used this feature to indicate that the fractures formed under relatively high differential stress.

3.2. Cementing material

The veins are mostly composed of calcite with occasional quartz. The original growth textures of the veins are well-preserved and exhibit comb structures with grain growth from the fracture walls towards the median line (Fig. 7a-c). The feature suggests that they formed as open fluid-filled fractures during extension events (e.g., Späth et al., 2022). Microscopic examination of the veins indicates that there was no shear displacement, and that they represent sites of dilation created by hydrolytic fracturing.

Optical observations of the veins indicate that the calcite grains grew perpendicular to the fracture walls towards the median line, forming a syntaxial texture (Fig. 7d-e). The elongate blocky or fibrous texture of the grains suggests that the growth of the carbonate was displacement-

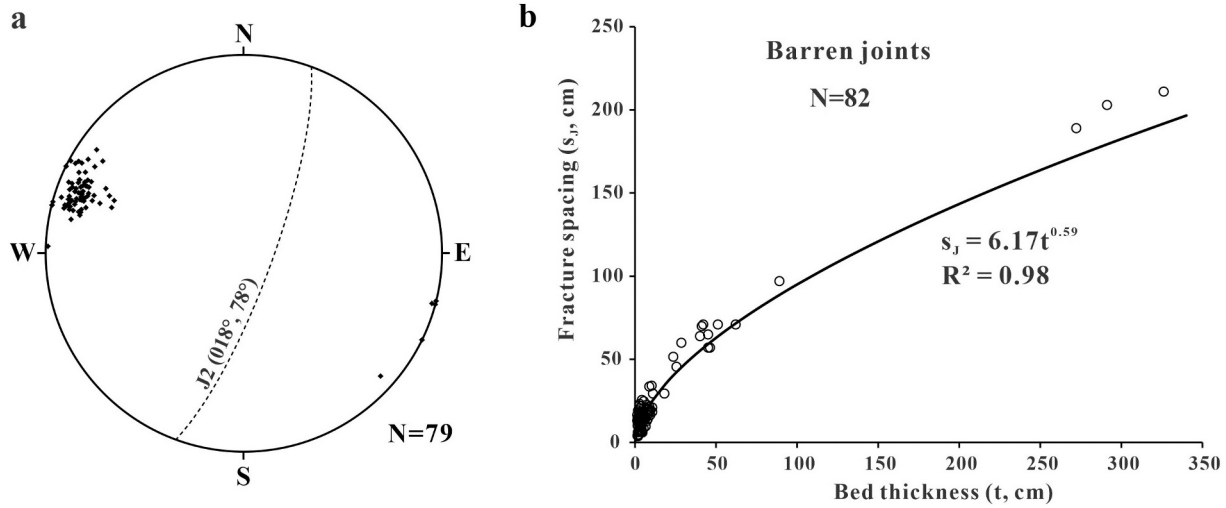

Fig. 2. Orientations (a) and plots of fracture spacing versus bed thickness (b) for non-cemented joints in graywacke beds at Ste-Anne-des-Monts, Quebec, Canada. The average attitude of the joints is (018°, 78°). N: number of measurements.

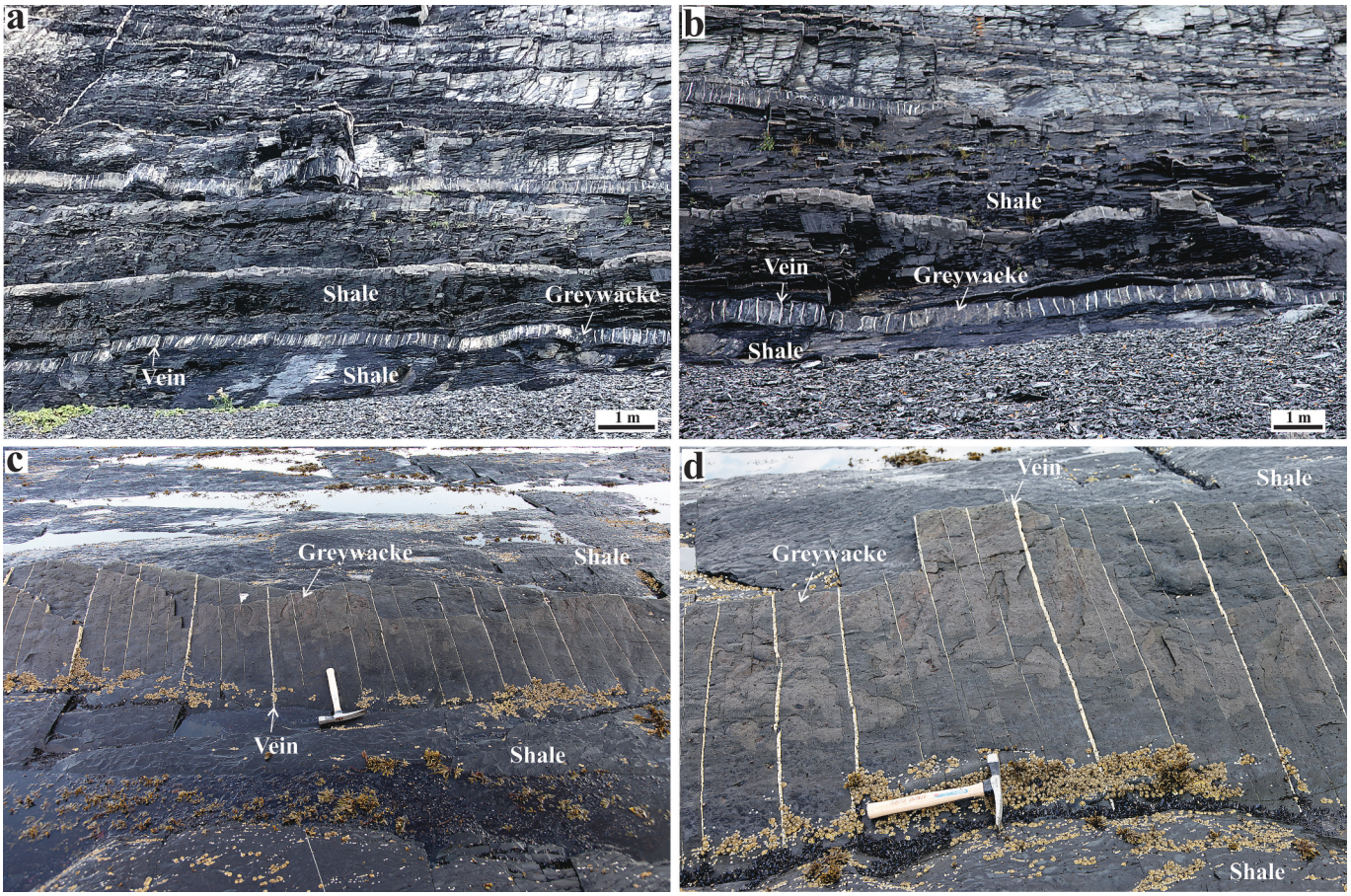

Fig. 3. Typical stratabound carbonate veins in graywacke beds from site 54 (a-b, cliff, GPS coordinates: 49°15′11.8" N, 65°31′19.9" W) and site 57 (c-d, wave-cut platform, GPS coordinates: 49°15′12.3" N, 65°32′30" W). The veins are commonly arrested at the upper and lower boundaries of graywacke (competent) beds and have rarely propagated into the shale (incompetent) layers. Hammer in (c-d) is 27.9 cm in length.

controlled rather than surface-controlled, with their long axes oriented perpendicular to the fracture walls. The microstructures of the veins such as wall-parallel inclusion bands, which are produced by recurrent crack-seal events due to repeated fluid pressure pulses, are rare except within some thick veins (w > 10 mm) (Ramsay, 1980; Stowell et al., 1999).

3.3. Estimate of extension strain

The extension strain (ε) of a fractured bed was estimated according to the sums of vein thicknesses ($W = \sum_{i=1}^{n} w_i$) and spacings ($S = \sum_{i=1}^{n} s_i$) which are measured along a scanline normal to the veins (e.g., Gross and Engelder, 1995):

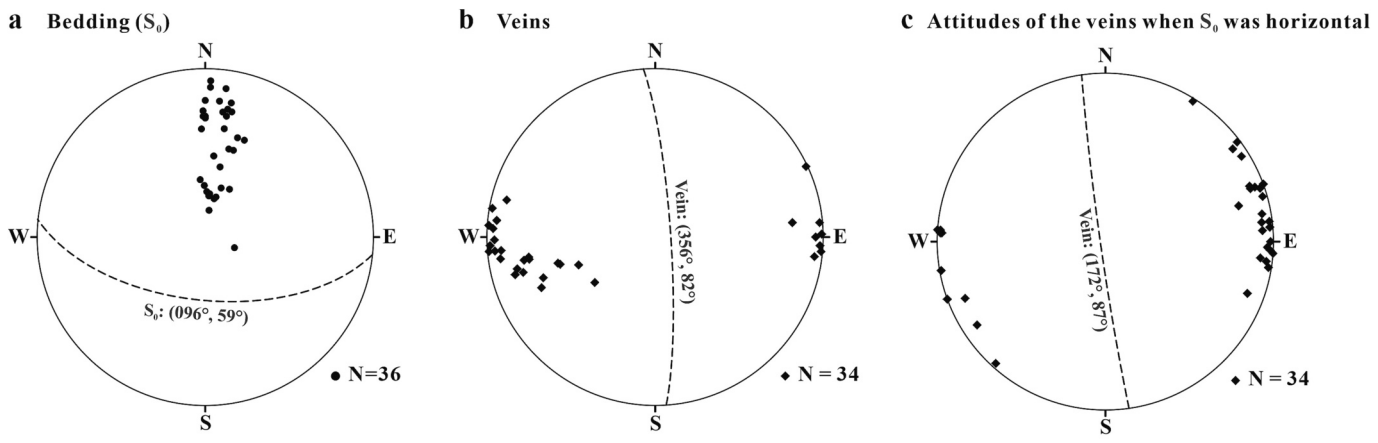

Fig. 4. Lower-hemisphere, equal-area projection of graywacke bedding planes (a) and planar veins (b-c). N: number of measurements. The best-fit plane for each diagram is shown as a dashed great circle.

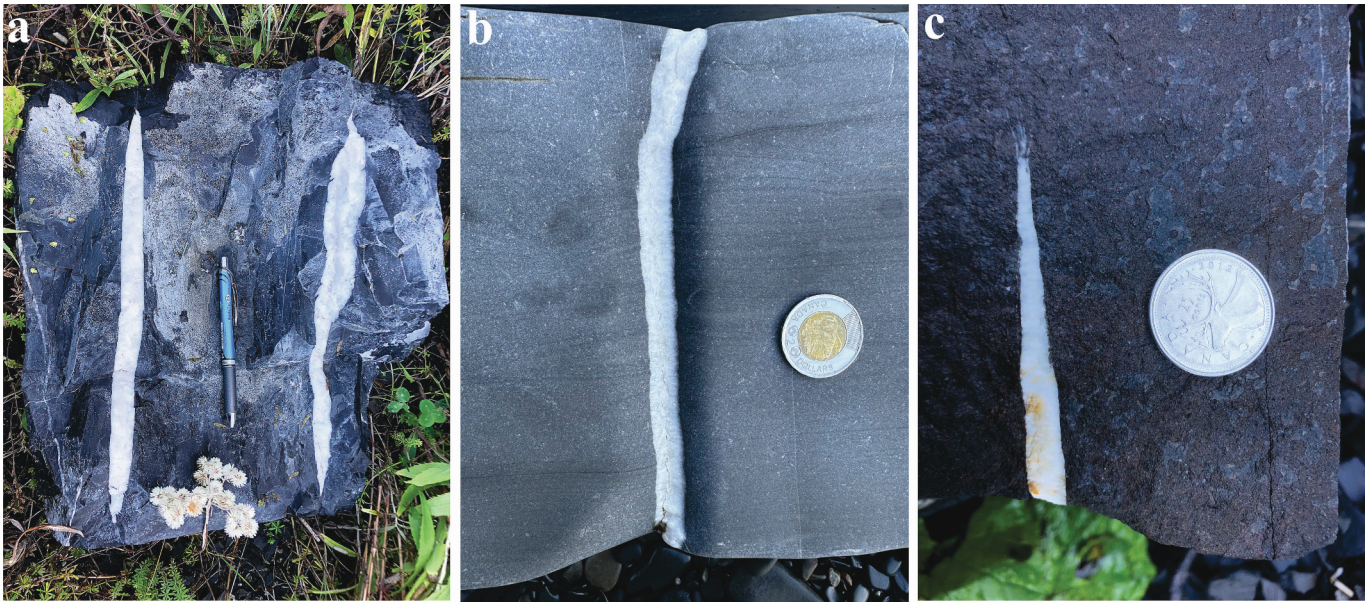

Fig. 5. Veins displaying three distinct shapes within the graywacke beds: lenticular (a), wall-parallel (b), and semi-lens (c). The pen in (a) measures 14 cm in length, while the coins in (b) and (c) have diameters of 23.88 mm and 28.00 mm, respectively.

$$\varepsilon = \frac{W}{(S+W)} \quad (1)$$

For each vein with a convex lens shape, we utilized the maximum thickness at the center of the vein. Strain measurements were conducted on 26 beds of continuous calcareous graywacke in the Rivière-à-Claude, Gros-Morne, Grande-Vallée, and Petite-Vallée regions. The layers exhibited strains ranging from 1.4% to 8.5%, with a mean of 3.8% (standard deviation of 1.67%, as shown in Table 1). These findings suggest that the graywacke beds have undergone crack-seal processes accommodating up to 8.5% of extension. These results are consistent with previous estimates from other regions (Bowyer and Kelly, 1995; Gross and Engelder, 1995; Gillespie et al., 1999; Hooker et al., 2014, 2018). However, it should be noted that the reversed strain calculated using Eq. (1) is only an estimation of the layer-parallel extension accommodated by bedding-normal veins within the fracturing beds. This strain is lower than the true strain of the bulk rocks, in which the soft shale layers were subjected to significantly greater deformation than the competent graywacke beds (Clyne and Withers, 1993; Zhao and Ji, 1997).

3.4. Vein thickness

Vein thickness or aperture was measured perpendicular to the walls, and the resulting histograms of measured thicknesses are presented in Fig. 8. The frequency distributions of vein thicknesses are positively skewed. A total of 1290 veins were measured from 26 beds of graywacke, and their thicknesses ranged from 1.0 mm to 9.1 cm with a mean of 8.4 mm (standard deviation: 7.5 mm), a median of 7.0 mm, and a mode of 3.0 mm. The relationship between mean vein thickness (w) and bed thickness (t) and vein-normal extension strain (ε) is plotted in Fig. 9a and b, respectively. The best fitting of the data yields:

$$w = 0.037\,t + 0.206 \quad (R^2 = 0.64) \quad (2)$$

and

$$w = 0.334\varepsilon - 0.151 \quad (R^2 = 0.55) \quad (3)$$

Fig. 6. Veins initiating from the lower boundary and then propagating towards the upper boundary of the graywacke layer (site 44, GPS coordinates: 49°13′17" N, 65°52′57" W). Hammer in (a and c) and pen in (b and d) are 27.9 cm and 14 cm in length, respectively.

for the graywacke, where both w and t are in cm and ε in %. Therefore, the data suggests a linear relationship between vein thickness and either bed thickness or extension strain. However, there is no apparent correlation between vein spacing (s) and thickness (w) as shown in Fig. S4.

The plots of logarithmic cumulative frequency versus logarithmic vein thickness consistently show concave-downward curves for the scaling data (Fig. S5). This clear non-linearity indicates that the vein thickness data from the Quebec Humber zone do not follow a power-law distribution (e.g., Gillespie et al., 1999; Fagereng, 2011), which is both factual and scale-invariant, within the range of vein thicknesses examined (Brooks Clark et al., 1995; Hooker et al., 2014; Gudmundsson, 2022). In a power-law distribution, the plot is linear with a slope of D in log-log space. If an important portion of the vein-induced extension strain is accommodated by the thinner veins rather than the thicker ones, $D > 1$ (Scholz and Cowie, 1990; Brooks Clark et al., 1995; Fagereng, 2011).

Previous studies (e.g., Gudmundsson, 1999; Philipp, 2012) have used the length/thickness ratios of mineral veins to estimate the magnitude of fluid overpressure. However, measuring the full length of a vein is only possible when both lateral ends are visible on the bedding plane, which is only the case for short veins. For long veins, one or both lateral ends may not be observable in the outcrops, and as a result, we did not attempt to measure the length/thickness ratios of mineral veins in the study region.

3.5. Vein spacing (s_v)

The spacing between adjacent veins in parallel is referred to as vein spacing (s_v). Vein spacing and its distribution are essential parameters for describing the spatial arrangement of veins (Van Noten and Sintubin, 2010; Marrett et al., 2018). From well-exposed coastal outcrops, 1650 vein spacing data from 41 calcareous graywacke beds have been measured. The thickness of the graywacke beds ranges from 2.4 cm to 283.0 cm with a mean of 35.4 cm (standard deviation: 49.3 cm). Each scanline was perpendicular to veins, and the accuracy of measurements is approximately 1 mm. The mean vein spacing of individual beds varies from 5.8 cm to 120.0 cm with a mean of 28.8 cm (standard deviation: 21.7 cm). The plots of logarithmic cumulative frequency versus logarithmic vein spacing persistently show concave-downward curves (Fig. S6). This suggests that the data of vein spacing from the study region, which are similar to those reported in Fagereng (2011) for the Chrystalls Beach Complex on the South Island of New Zealand, do not follow a power-law distribution (Hooker et al., 2014).

Fig. 10 illustrates typical histograms of vein spacings measured in the study area. Among the 26 layers with >20 measured veins, the data of 9 are best-fit by the Gamma distribution, 7 by the lognormal distribution, 6 by the Weibull distribution, 2 by the Normal distribution, 1 by the logistic distribution, and 1 by the log-logistic distribution (Table S1). The exponential function did not provide a good fit to the vein spacing data. The best-fitting distribution was determined based on the KS-*p* value (*p*-value of Kolmogorov-Smirnov test). Among the 7 beds with >80 measured veins, the best fitting functions were Gamma (5 beds) and Weibull (2 beds). It is interesting to note that both the Weibull and Gamma distributions are special cases of the generalized gamma function, which describes a continuous probability distribution with three parameters. The Weibull distribution is a particular type of the generalized gamma distribution with the same shape parameter.

The regularity of fracture spacing can be quantified using the

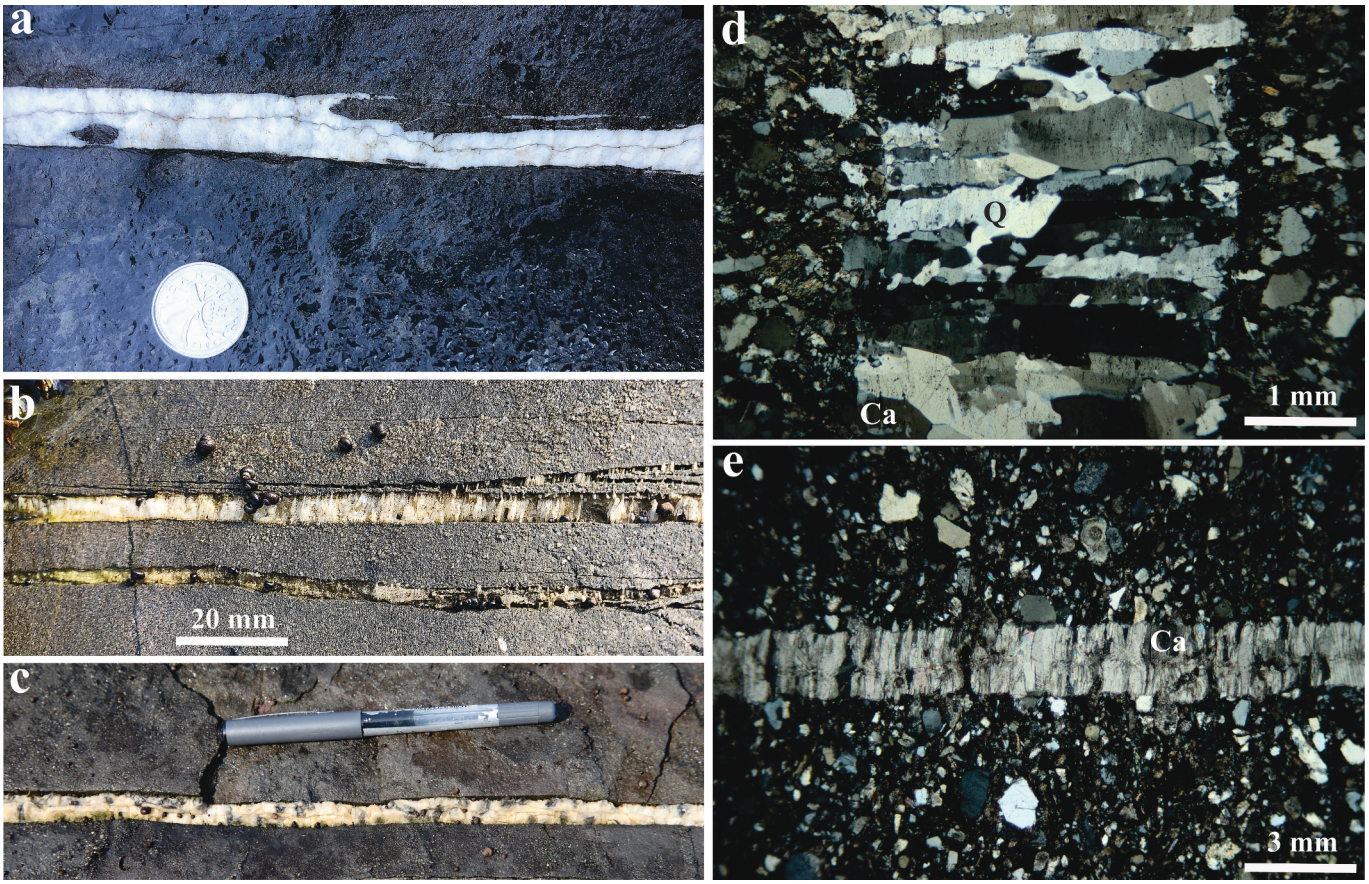

Fig. 7. Outcrop (a-c) and optical (d-e) photographs showing internal structures of veins. The cementing mineral is generally calcite although quartz occasionally occurs. Elongate crystals are oriented approximately perpendicular to the vein walls, indicating that the fractures were opened in a direction normal to their walls. Coin in (a) has a diameter of 23.88 mm, and pen in (c) is 14 cm in length.

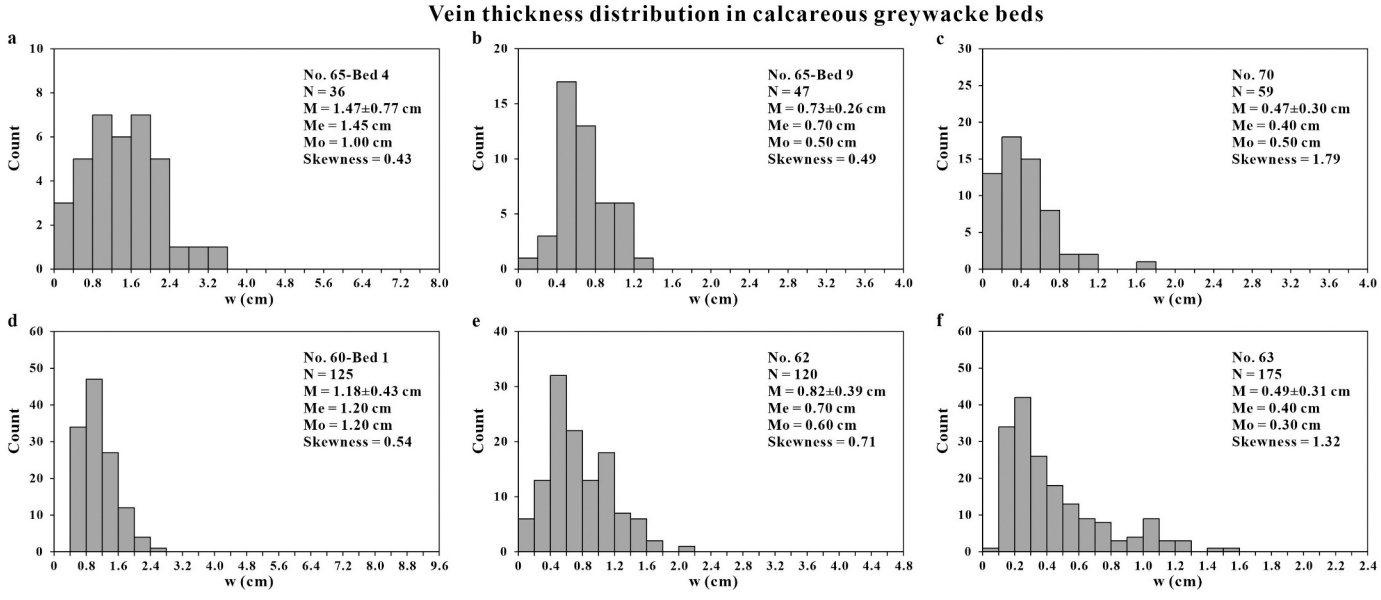

Fig. 8. Typical histograms for vein thickness data measured in each continuous graywacke bed. N, the number of measurements; M, the arithmetic mean; Mo, the mode (the most frequently occurring value in the distribution); Me, the median (the 50th percentile in the distribution).

coefficient of variation (C_v), which is the ratio of the standard deviation to the mean value (Gillespie et al., 1999, 2001; Fagereng, 2011). When vein spacings are periodically spaced, $C_v = 0$ (s_v is a constant), whereas $C_v = 1$ when vein spacings display a Poisson's distribution. When veins are anti-clustered, or regularly spaced, $C_v < 1$, and $C_v > 1$ when veins are clustered. Among the 41 beds of calcareous graywacke from which vein spacing measurements were taken (Table 1), C_v ranges from 0.19 to 0.66 with an average of 0.394 ± 0.102 (standard deviation), indicating that

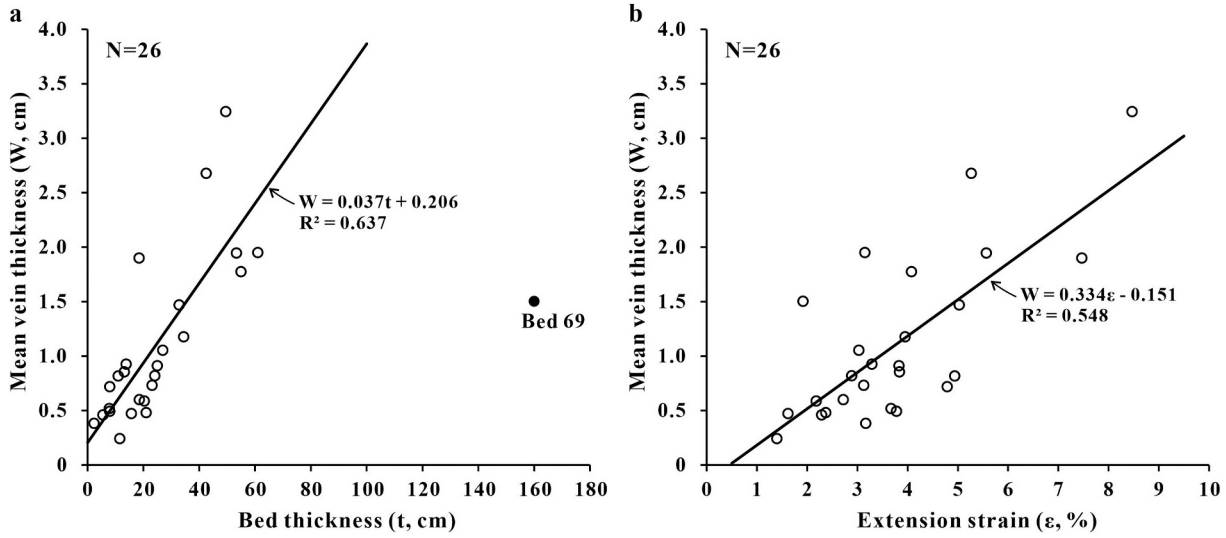

Fig. 9. Plots of mean vein thickness versus bed thickness (a) and layer-parallel extension strain (b) for 26 graywacke layers.

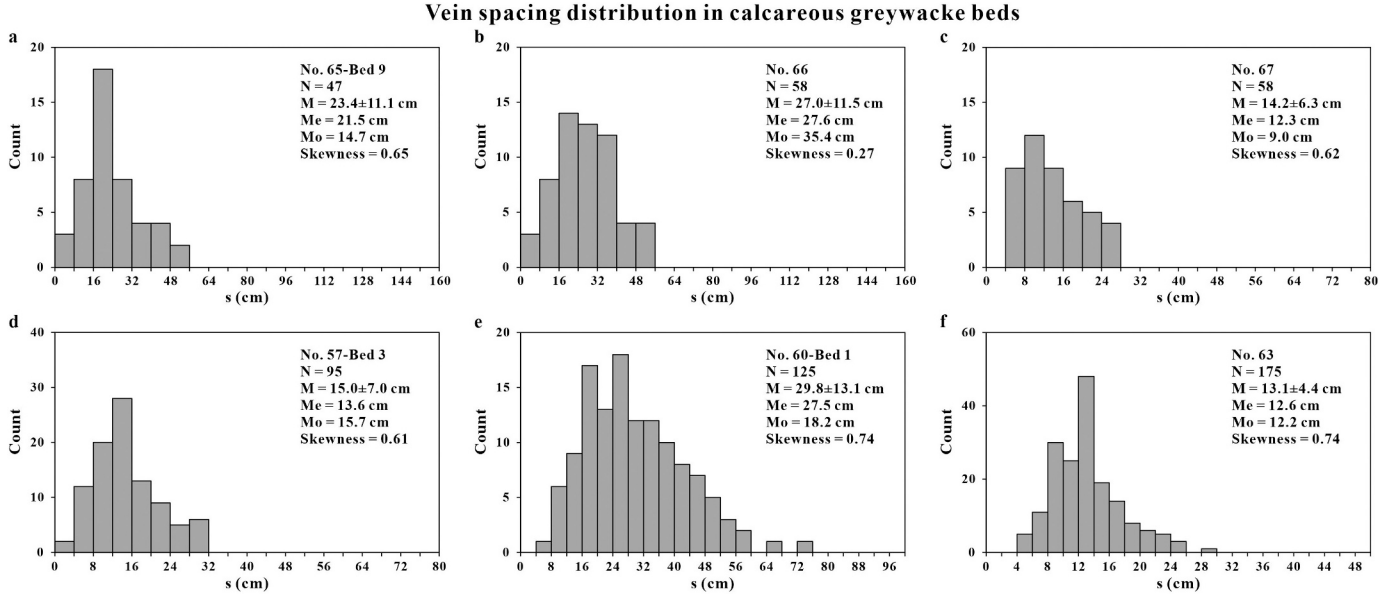

Fig. 10. Typical histograms for vein spacing data measured in each continuous graywacke bed. N, the number of measurements; M, the arithmetic mean; Mo, the mode (the most frequently occurring value in the distribution); Me, the median (the 50th percentile in the distribution).

the vein spacings are regularly spaced or anti-clustered. The Gaspésie veins exhibit different clustering behavior compared to the Cappanawalla veins, which have a high degree of clustering ($C_v > 1$) attributed to the presence of faults (Gillespie et al., 2001).

3.6. Relation between bed thickness (t) and vein spacing (s_v)

Veins, as documented in drill cores with a diameter of several centimeters (e.g., Hooker et al., 2017), make it difficult to measure the s_v-t relationship because the spacing between veins, which depends on the thickness of the beds, is generally much larger than the diameter of the core. However, the wave-cut platforms along the south shore of the Saint-Lawrence River provide excellent continuous outcrops of interlayered sedimentary rocks that allow for the study of the s_v-t relationship. Figs. 11a-c show plots of vein spacing (s_v) versus bed thickness (t) for 41 graywacke beds. The s_v-t data from the Humber zone (Fig. 11) can be fitted according to linear (Narr and Suppe, 1991; Ji and Saruwatari, 1998; Van Noten and Sintubin, 2010; Rustichelli et al., 2013; Levi et al., 2019), power-law (Ji et al., 2021) and Michaelis–Menten (Ji, 2022) equations:

$$s_v = 0.41\,t + 14.17 \tag{4}$$

$$s_v = 3.81\,t^{0.60} \tag{5}$$

$$s_v = \frac{164.5t}{141.1 + t} \tag{6}$$

where both t and s_v are in cm. The correlation coefficients (R^2) for Eqs. (4), (5) and (6) are 0.88, 0.92 and 0.96, respectively. The linear equation showed a significantly lower goodness-of-fit compared to the non-linear functions.

Eq. (6) possesses a form of the Michaelis–Menten equation (Michaelis and Menten, 1913):

$$s = \frac{\alpha t}{\beta + t} \tag{7}$$

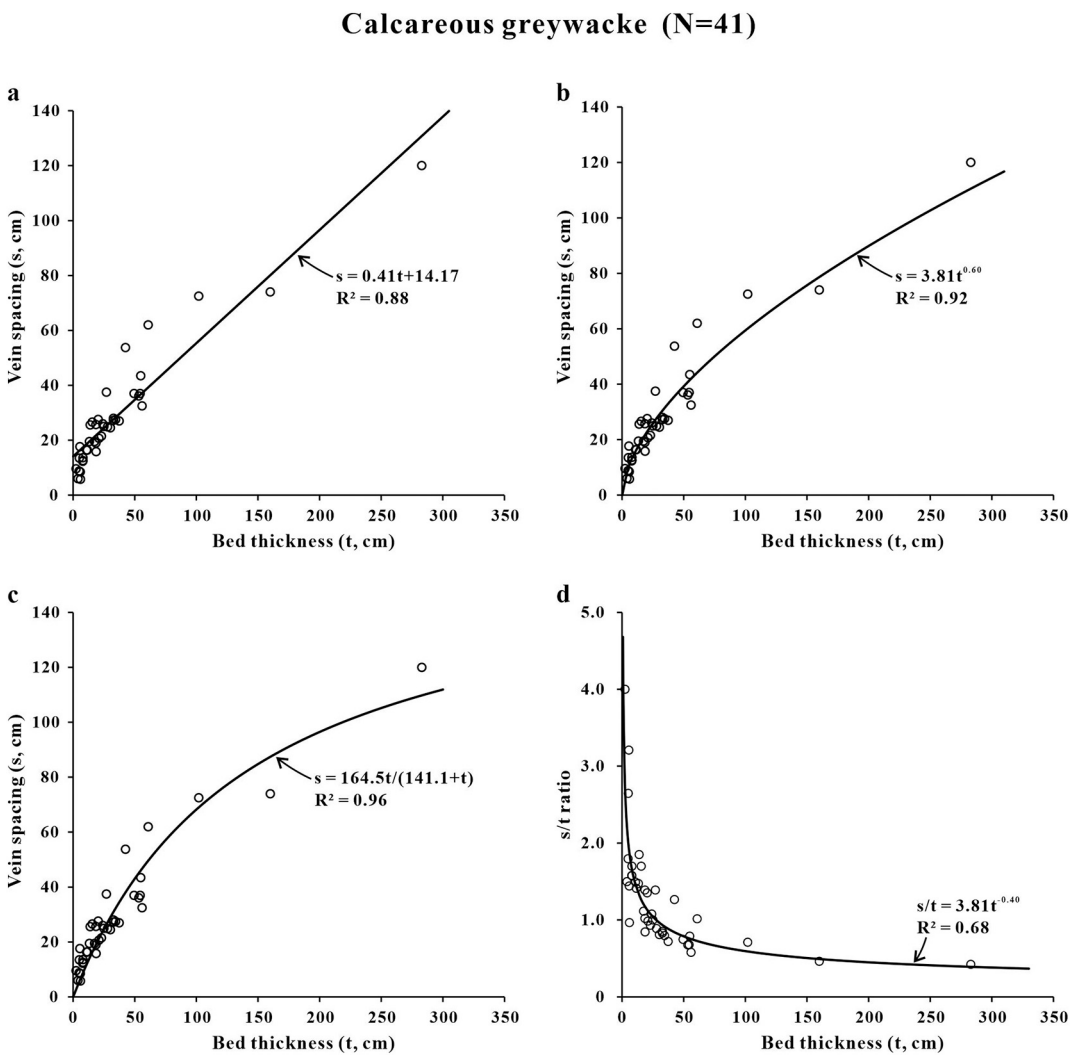

Fig. 11. Plots of vein spacing (a-c) or s/t ratio (d) versus bed thickness for 41 graywacke layers. The data are best-fitted using linear (a), power-law (b and d) and Michaelis–Menten (c) equations.

where α is the maximum fracture spacing which is no longer affected by an increase in bed thickness (t) and β is the bed thickness at which $s = 0.5\beta$. For the graywacke beds in the Quebec Humber zone, α = 164.5 cm, and β = 141.1 cm. The geological applications of the Michaelis–Menten equation have been described in Angelier et al. (1989), Souffaché and Angelier (1989) and Ji (2022).

4. Numerical modeling

We conducted a series of 2D finite element models using a code named RFPA (Rock Failure Process Analysis) to investigate the impact of the strength recovery coefficient (δ) on fracture spacing in a brittle bed located between upper and lower soft, elastoplastic matrix layers. RFPA is a rock failure analysis package code based on the finite element method. It has been extensively utilized since 1997 (Tang, 1997) in various numerical studies related to rock mechanics, mining, geotechnical engineering (e.g., Tang et al., 2006; Chen et al., 2022; Gong et al., 2022), and geological sciences (Tang et al., 2008, 2020; Heap et al., 2014; Wasantha et al., 2014; Griffiths et al., 2017; Pakzad et al., 2018). Detailed information about the method's principles can be found in these earlier papers. The RFPA method offers several advantages compared to previous numerical methods (e.g., Gross et al., 1995; Bai et al., 2002; Chemenda et al., 2021; Chemenda, 2022) used for simulating tensile fractures in layered rocks. These advantages include: (a) Consideration of heterogeneity in material strength parameters: The RFPA method accounts for variations in the strength properties of the materials involved, acknowledging their heterogeneity. (b) Introduction of elastic modulus reduction for failed elements: In the RFPA method, the elastic modulus of failed elements is reduced accordingly. (c) Progressive recording of the event-rate of failed elements: The RFPA method allows for continuous recording of the rate at which elements fail during the simulation. (d) Consideration of the degradation of material properties during the deformation process: The RFPA method incorporates damage mechanics to represent the degradation of material properties as deformation progresses, resulting in a more realistic representation of the fracture process. In addition, the RFPA method is based on the unit element, ensuring consistency in the fracture strength criterion.

Each model used in our study has dimensions of 40 cm by 12 cm and is subjected to continuous longitudinal extension. The model comprises a brittle competent bed sandwiched between two unbreakable elasto-viscoplastic incompetent layers. The central bed is 3 cm thick and possesses a Young's modulus (E) of 50 GPa, a Poisson's ratio (ν) of 0.25, a tensile strength (C) of 10 MPa, and a compressive strength of 100 MPa. The upper and lower layers, each 4.5 cm thick and with E = 10 GPa and ν = 0.35, exhibit elasto-viscoplastic behavior. These layers deform elastically and viscoplastically below and above the yield point, with a flow strength equal to the yield strength. The residual strength

coefficients for the competent and incompetent layers are 0.1 and 1, respectively.

The coefficient δ represents the ratio of the strength (e.g., tensile strength) and elastic modulus (e.g., Young's modulus) of the sealing material (e.g., polycrystalline calcite) to those of the host rock. $\delta = C_s/C_h = E_s/E_h$ if $C_s/C_h < 1$, where C is the tensile strength, E is the Young's modulus, and subscripts s and h represent the sealing material and the host rock, respectively. If the joint is barren with no cementation, $\delta = 0$ (zero cement case). However, $\delta = 1$ if $C_s/C_h = E_s/E_h \geq 1$ because the cement adhesion to the fracture walls cannot exceed the tensile strength of the host rock, even if the cement is stronger. Therefore, δ cannot be >1, and it ranges between 0 and 1 for the following reasons: (1) incomplete sealing of fractures (e.g., Shang et al., 2016; Späth et al., 2022), (2) weak adhesion between the cement and the host rock (e.g., Virgo et al., 2014), (3) lower strength of the cement compared to the host rock (Gale and Holder, 2010), and (4) fracturing in the host material immediately in contact with the cementing material if the latter is mechanically stronger.

To account for the inhomogeneity in the layers, we utilize Weibull parameters. We set m = 2.5 and m = 6.0 for the competent and incompetent layers, respectively, as suggested by Tang et al. (2008). These parameters capture the statistical variability of fracture strength within the bed, which arises from its inherent heterogeneity (Weibull, 1952). The presence of mechanical heterogeneity leads to stress fluctuations about the mean stress of a homogeneous material. Local stresses dictate the nucleation and propagation of fractures, which in turn affect the distribution of fractures in the material. When a material is heterogeneous, the standard deviation of fracture spacing is typically larger than that in a homogeneous material (e.g., Fischer and Polansky, 2006).

In our study, we investigate the effects of crack healing or cement precipitation sealing on the mechanical behavior of the models. Specifically, we simulate the restoration of tensile strength and Young's modulus in broken elements to different percentages of the host rock's strength. We consider four scenarios, which we call models 1, 2, 3, and 4. In model 1, we restore the tensile strength and Young's modulus of broken elements to 0% of the host rock's strength. In model 2, we restore these to 50%. In model 3, we restore these to 75%. In model 4, we restore these to 100%. We keep all other model parameters constant throughout these simulations. Models 1 and 4 represent two end-members of our study. In model 1, broken elements are not healed or sealed, which leads to the formation of barren joints. In model 4, broken elements are fully healed or sealed after the crack extends to both the upper and lower interfaces of the brittle layer. The sealing results in the formation of veins that have identical mechanical properties to the host rock. To avoid any effects from the ends of the models, we exclude fractures that occur within 5 cm of each end in each run.

We have successfully replicated the ongoing processes of fracture initiation, propagation, infilling, and increased fracture density in sedimentary rock layers by considering material heterogeneity, including strength and flaws, and the recovery of strengths and elastic moduli due to fracture healing or sealing (Audio S1). It should be noted that our modeling did not take into account the portion of vein-related extension strain that is accommodated by the insertion of veins, and for simplicity, we assumed that each vein has a thickness equivalent to that of a single mechanical element. Our modeling has shown that:

1. Fracture initiation can occur from either the interfaces or the interior of the layer. Fractures initiated at the interface propagate perpendicularly towards another interface, while fractures initiated in the center of the layer propagate vertically towards the upper and lower boundaries of the layer. Fractures typically terminate at the interfaces without propagating into the adjacent soft layers, which is consistent with our field observations (Fig. 3, Fig. S2).

   Fracture initiation can occur from either the interfaces or the interior of the layer. Fractures initiated at the interface propagate perpendicularly towards another interface, while fractures initiated in the center of the layer propagate vertically towards the upper and lower boundaries of the layer. Fractures typically terminate at the interfaces without propagating into the adjacent soft layers, which is consistent with our field observations (Fig. 3, Fig. S2).
2. Unlike the shear-lag model that predicts mid-point fracturing in fully homogeneous materials (Hobbs, 1967; Masuda and Kuriyama, 1988; Ji and Saruwatari, 1998), our numerical modeling shows that layer-normal fractures randomly occur in the brittle layer (Fig. 12). Even between two existing fractures, a new fracture can form unnecessarily at the middle point (Fig. 12) if it nucleates at a point where the local stress attains the local element failure strength.
3. Fractures commonly propagate in relatively straight directions that are approximately perpendicular to the layer because each fracture initiates at a single failed element and then grows perpendicularly to the local minimum principal stress (Audio S1).
4. As the tensile strain gradually increases, stress is transferred from the upper and lower incompetent layers to the central competent bed through interfacial adhesion. If the accumulated tensile stress surpasses the local tensile strength of the brittle bed, a fracture will occur at that position and propagate until it reaches the upper and lower interfaces. The occurrence of local fractures relieves stress, leading to the concentration of new high tensile stress between adjacent fractures. If the strength criterion continues to be met, new fractures will form and fill the gaps between existing fractures, thereby reducing the fracture spacing until fracture saturation is achieved. Some fractures may extend into the matrix due to ongoing loading after reaching fracture saturation.
5. The fracture spacing shows a nonlinear decrease with increasing extension strain (up to 0.23%), which can be described by a power law equation (Fig. 13). Importantly, the fracture spacing (Fig. 13a) or the s/t ratio (Figs. 13b and 14) at a given strain decreases with increasing the strength recovery coefficient of fractures. The strength recovery achieved by crack healing or mineral precipitation sealing (formation of veins) results in a closer final fracture spacing. At the extension strain of 0.1%, for example, veins have a closer fracture spacing than barren joints under the same conditions (Figs. 13-14). The healed or sealed cracks or veins are not re-cracked in the model with δ = 100% (Fig. 12d). However, partially recovered fractures or veins [models with δ = 75% (Fig. 12c) and particularly δ = 50% (Fig. 12b)] can be re-cracked because the veins are mechanically weaker than the host rock. This is consistent with previous results of numerical simulations (Hooker and Katz, 2015; Virgo et al., 2014; Späth et al., 2022) and laboratory experiments (Lee et al., 2015; Shang et al., 2016) that weaker cement produces remarkable re-cracking. Interestingly, re-cracking of extant veins does not decrease the vein spacing (Figs. 12-13) although it may increase vein thickness in a real geological setting.
6. The fracture patterns produced by all simulations are regularly spaced, as the C_v values (standard deviation divided by mean) are consistently <0.75. The maximum C_v value (0.71) emerges at δ = 0%, while C_v = 0.54 at δ = 100%. Thus, veins are not only more closely but also more regularly spaced than joints, indicating the mechanical effect of cementation on fracture patterns.

5. Discussion

5.1. Origin of the veins

Previous studies (Gillespie et al., 1999; Stowell et al., 1999; Fagereng, 2011; Passchier and Trouw, 2005) have shown that veins developed in metamorphic rocks under greenschist-facies conditions often exhibit complex and irregular shapes with multiple segments and a network-like pattern, and they are typically non-stratabound. These veins in metamorphic rocks also display power-law distributions for thickness and spacing, with a characteristic clustering tendency ($C_v > 1$). In contrast, the veins observed in the sedimentary strata of the Quebec Humber zone

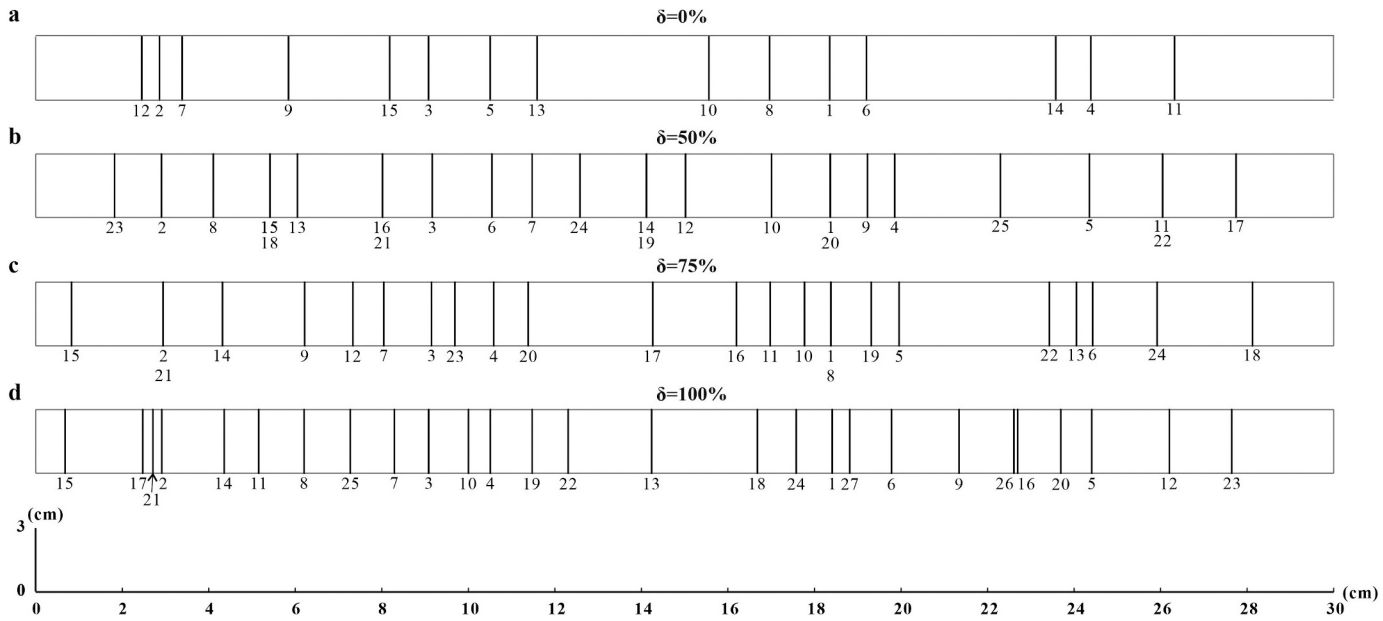

Fig. 12. Sequential formation of tensile fractures in the central brittle layer (3 cm thick and 30 cm long) of each model with the strength recovery coefficient of 0% (a). 50% (b), 75% (c) and 100% (d). The numbers indicate the order of fracture formation.

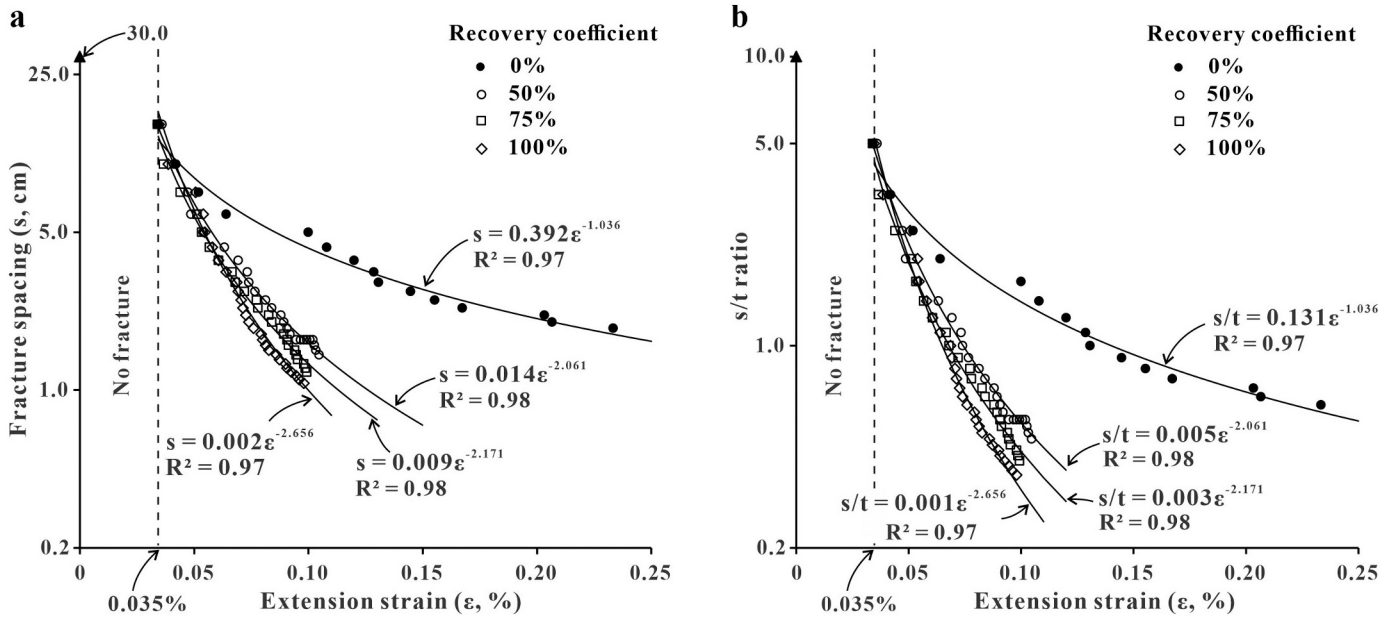

Fig. 13. Numerical modeling results showing the effect of the strength recovery coefficient (δ) on the fracture spacing (a) and s/t ratio (b) with increasing the layer-parallel extension strain. The brittle layer does not crack until a critical extension strain has been achieved.

are primarily stratabound and have simple planar shapes (Fig. 3). The stratabound veins in sedimentary rocks do not exhibit power-law distributions for thickness or spacing (Figs. S5, S6). Additionally, these veins are regularly spaced, which is indicated by low C_v values ranging from 0.19 to 0.66, with an average of 0.39. The aforementioned differences between metamorphic rocks and sedimentary rocks suggest potential variations in their formation mechanisms under different deformation and environmental conditions.

The fibrous cements, when present, are approximately perpendicular to the vein margin or fracture wall, suggesting that the veins were formed by extensional opening mode fractures rather than hybrid (extension-shear) fractures. This interpretation is supported by the lack of slickensides-bearing vertical veins. In addition, the presence of angular wall rock microblocks (breccia) within some veins indicates that fracture opening and mineral precipitation occurred rapidly, possibly due to hydraulic bursting caused by a sudden drop in fluid pressure. According to Tinni et al. (2019) and Gudmundsson (2022), hydraulic fractures can propagate at speeds close to S-wave velocity. Since the aqueous fluid has a very low viscosity, unlike granitic magma, the fluid front can move as fast as the fracture front, allowing the fluid pressure to be maintained at the fracture tips. If this scenario holds true, there should be minimal time delay between the advancement of the fluid front and the fracture front during the formation of veins in relatively porous and permeable sedimentary rocks.

The microstructures of veins in the Quebec Humber zone (Fig. 7) suggest that mineralized precipitation occurred during layer-parallel

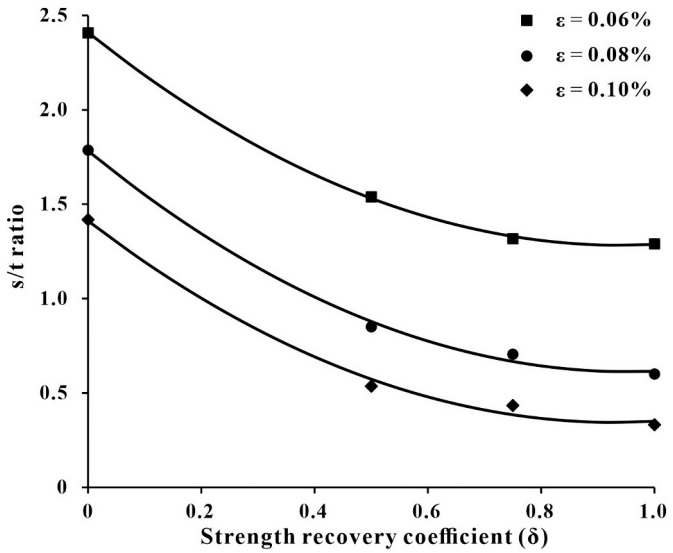

Fig. 14. Numerical modeling results showing the variation of the ratio of fracture spacing to bed thickness (s/t) as a function of strength recovery coefficient (δ) at three different extension strains (a: 0.06%; b: 0.08%; c: 0.10%).

extension-induced crack opening. The calcite crystals at vein margins generally display a fine-grained texture because they nucleated on small calcite grains in the calcareous greywacke. Importantly, microstructural evidence suggests that each individual vein resulted essentially from a single crack-seal event, which explains that their apertures are relatively thin (~7 mm). Evidence of cements repeatedly breaking due to multiple, periodic crack-seal events is found only in relatively wide veins (>10 mm) that have been widened by multiple crack-seal events.

The structures shown in Fig. 6 suggest that tensile fractures initiated at the lower boundary of the graywacke bed and propagated approximately upward. Due to the pressure gradient in the vertical direction, fluids derived from diagenesis of sediments (compaction, densification, and metamorphic dehydration) were transported upward from depth into newly developed opening fractures. Mineral precipitation appears to have occurred simultaneously or immediately after the opening of the fracture. If the vertical cracks were progressively filled by mineral precipitation, the veins might exhibit a colloform texture formed during sequential stages of precipitation from bottom to top. Few voids or cavities would appear at the top of the crack if it had been partially filled by cement under the influence of gravity. Our observations do not support the assumption that fractures remained open and fluid-filled for a long period of time (Brooks Clark et al., 1995).

The bed-parallel shear veins, characterized by slickensides, differ from extension veins, which were opened by vertical extension before filling, although both types of veins are horizontally aligned (Sibson et al., 1988; Philipp, 2008). Flat-lying extension veins require pore fluid overpressure (i.e., local fluid pressure exceeding overburden pressure, Sibson et al., 1988; Gillespie et al., 2001) for formation. As depicted in Fig. S2, the graywacke layer comprises closely spaced, layer-bound veins perpendicular to bedding. Cross-cutting relationships indicate that bed-parallel veins formed concurrently with bed-normal veins. Bedding-parallel veins were resulted from interfacial slip-induced delamination occurring at large extension strains, as suggested by the presence of small vein spacings (Fig. S2). This interpretation agrees with previous analytical (Ji et al., 1998; Schöpfer et al., 2011), numerical modeling (Cooke and Underwood, 2001; Tang et al., 2008; De Joussineau and Petit, 2021), and experimental (e.g., Morrison et al., 1988; Tripathi and Jones, 1998) results. Bedding-parallel veins are reliable indicators of interfacial slip and delamination between beds with differing mechanical properties during bed-parallel extension. Interfacial delamination indicates that the vertical layer-bound veins have reached saturation, as it reduces the layer-parallel tensile stress between adjacent opening fractures and thereby prohibits further fracture infilling (Ji et al., 1998; Chang et al., 2017).

5.2. Implications of the s_V-t relation for strength recovery by mineral precipitation

Previous numerical models by authors such as Fischer et al. (1995), Gross et al. (1995), Bai and Pollard (2000), Bai et al. (2002), Korach and Keer (2002), and Li and Yang (2007) only computed the distribution of layer-parallel normal stress between two precut, through-going cracks and did not provide information about fracture initiation, propagation, strength recovery, and infilling. However, our numerical models, which consider the effects of material heterogeneity (including strength and flaws) and crack healing or sealing (mineral precipitation), have successfully replicated the formation processes of joints (δ = 0%) and veins (δ = 50%, 75%, and 100%). The resulting fractures (Audio S1) exhibit regular shapes that strongly resemble the natural joints or veins typically found in layered sedimentary rock beds. Our modeling further demonstrates that, relative to joint spacing, vein spacing is more uniformly spaced. This finding (Figs. 12-13) is consistent with our field observations (Figs. 2b, 11b, and unpublished data from St-Jean-Port-Joli) and can be explained by the most straightforward mechanical analysis presented below.

When a mode I opening fracture has formed, the barren joint plane becomes a free surface on which neither tensile nor shear stress can be transferred. In the brittle layer shown in Fig. 15a, the tensile stress (σ) built up to the right of the barren joint will not be able to transfer to the left side. The formation of a potential fracture will be controlled mainly by the shear stresses (τ) transferred from the ductile (non-fracturing) matrix. The relation between joint spacing (s_J) and bed thickness (t) after a fracture saturation has been achieved has been expressed by a simple equation (Lloyd et al., 1982; Price and Cosgrove, 1990; Ji et al., 1998; Ji et al., 2021):

$$2\tau s_J = Ct \tag{8}$$

then,

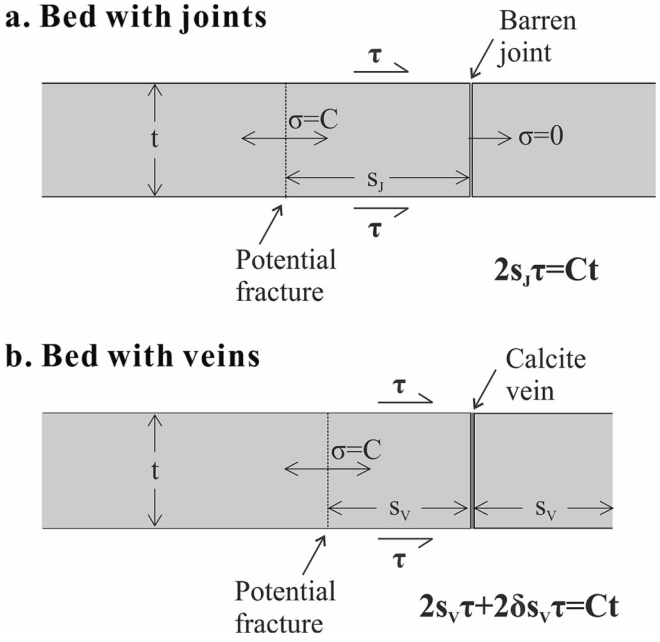

Fig. 15. Schematic illustration of the mechanical equilibrium analysis for a brittle layer embedded in a ductile matrix. (a) Barren and (b) cemented fractures. Variables are defined in the text.

$$s_J = \frac{C}{2\tau}t \tag{9}$$

where τ is the interfacial shear stress between the strong and weak beds, and C is the tensile strength of the strong bed. Eq. (9) represents the mechanical balance that occurs when a new fracture segment forms in a competent bed that is surrounded by ductile, incompetent beds. The tensile stress in the competent bed is generated by the shear stresses (τ) acting along the interfaces between the competent and incompetent beds. However, the maximum interfacial shear stress may not exceed the shear flow strength of the upper and lower layers, which undergo ductile deformation. When considering characteristic fracture spacing in layered rocks, the interfacial shear strength can be approximated as the shear flow strength of mudstone or shale.

The joints are unsaturated when $s_J < [C/(2\tau)]t$. With increasing layer-parallel extension, s_J progressively reaches to the value of $[C/(2\tau)]t$. The s_J is the joint spacing at the state of fracture saturation considering the presence of mechanical inhomogeneity in natural rocks. Each new crack results in locally relieving tensile stress. In the absence of cement precipitation or healing, relieved stress prohibits nearby crack initiation (Hooker and Katz, 2015) and a regular joint spacing as a function of bed thickness occurs according to Eq. (9). Eq. (9) implies that the s_J-t relation is C/τ ratio dependent. The joint spacing increases with raising the bed tensile strength (C) but lessens with increasing the shear flow strength of the incompetent layer (τ).

However, when an existing joint is healed or cemented through mineral precipitation to form a vein, traction can be restored across it with further extension of the layer (Fig. 15b). This is because the tensile stress is transferred from the interfacial stresses between the stiff and soft layers on either side of the vein. The variation of vein spacing (s_v) with bed thickness (t) can be described by

$$2\tau s_V + 2\delta\tau s_V = Ct \tag{10}$$

then,

$$s_V = \frac{C}{2(1+\delta)\tau}t \tag{11}$$

where δ is the coefficient of strength recovery by crack healing or sealing.

According to Carpinteri and Chiaia (1996), Bažant (2000), Paterson and Wong (2005) and Askeland et al. (2010), the size effect on the tensile strength of a brittle bed can be described by a power law:

$$\frac{C}{C_0} = \left(\frac{t}{t_0}\right)^{-1/k} \tag{12}$$

where C_0 is the tensile strength of the strong layer with a reference thickness of t_0, and k is the Weibull modulus of the strong layer (Weibull, 1952; Lawn, 1995; Bažant, 2000). Incorporating Eq. (12) into Eqs. (9) and (11), we obtain:

$$s_J = \frac{C_0}{2\tau}\left(\frac{t}{t_0}\right)^{-1/k}t \tag{13}$$

and

$$s_V = \frac{C_0}{2(1+\beta)\tau}\left(\frac{t}{t_0}\right)^{-1/k}t \tag{14}$$

where s_J and s_V are the joint spacing and vein spacing, respectively. Since the reference thickness of t_0 is adjustable and can be taken as unity, Eqs. (13) and (14) can be simplified, respectively, as

$$s_J = Mt^n \tag{15}$$

and

$$s_V = \frac{M}{(1+\delta)}t^n \tag{16}$$

with

$$M = \frac{C_0}{2\tau} \tag{17}$$

and

$$n = 1 - \frac{1}{k} \tag{18}$$

The graywacke-shale strata exposed in the Gaspésie region, including Ste-Anne-des-Monts, Rivière-à-Claude, Gros-Morne, Grande-Vallée, and Petite-Vallée, exhibit the same deformation pattern of north-verging, asymmetrical folds with subhorizontal hinges (Ji et al., 2021). In these strata, brittle structures are observed as barren joints in Ste-Anne-des-Monts and as veins in Rivière-à-Claude, Gros-Morne, Grande-Vallée, and Petite-Vallée. Both the joints and veins have a similar N-S strike and an average dip angle of 80°. The reason why the graywacke beds in the region of Ste-Anne-des-Monts developed barren joints instead of veins can be explained by the absence of $CaCO_3$-saturated fluids. The fluid that assisted in the fracturing of the graywacke beds contained very low concentrations of $CaCO_3$, and thus no mineral precipitation occurred along the open fractures to form veins.

Plots of fracture spacing (s_J) versus bed thickness (t), measured from 82 graywacke beds from Ste-Anne-des-Monts are illustrated in Fig. 2b, yielding a non-linear relationship for the barren joints:

$$s_J = 6.17\ t^{0.59} \qquad \left(R^2 = 0.98\right) \tag{19}$$

Comparison of Eq. (19) with Eq. (15) and Eq. (5) with Eq. (16) allows for the determination of the parameters: $n = 0.59–0.60$, $M = 6.17$, $\delta = 6.17/3.81–1 = 0.60$, and the Weibull modulus $k = 2.5$ for the graywacke beds. The calculations suggest that carbonate cementation resulted in a strength recovery coefficient of 60% relative to the original strength of the host bed. This δ value may be due to incomplete sealing (porosity in vein), a weak bond between the cement and host rock, and/or a weaker strength of the polycrystalline calcite cement compared to the host rock, which is predominantly composed of quartz, feldspar, and calcite.

The Weibull modulus, also known as the material mechanical heterogeneity index, is a shape coefficient of the distribution function that reflects the level of uniformity of a material in terms of its mechanical properties (Weibull, 1952; Tang et al., 2008). The higher the value of the Weibull modulus k, the more homogeneous the material is. However, few measurements of the Weibull modulus have been conducted on natural rocks. For instance, calcite marbles typically have Weibull moduli between 2.0 and 2.9 (Wong et al., 2006), while quartzites have a Weibull modulus of 4.2 (Lobo-Guerrero and Vallejo, 2006). Based on the field data collected, the obtained value of the Weibull modulus for the calcareous graywacke beds falls between that of the marble and the quartzite, suggesting that the rock is primarily composed of quartz and calcite.

According to Souffaché and Angelier (1989),

$$C = \left(\frac{\nu\rho g E\alpha}{2\pi}\right)^{1/2} \tag{20}$$

where E, ν and ρ are the Young's modulus, Poisson's ratio and density of the brittle fracturing layer, respectively, g is the gravitational acceleration, and α is described in Eq. (7) and equals 164.5 cm for the study area. Based on the parameters $\rho = 2.722$ g/cm^3, $E = 50$ GPa, and $\nu = 0.25$, the graywacke's tensile fracture strength (C) was calculated using Eq. (20) to be 9.3 MPa. This value, which was obtained from field-collected s-t data, falls within the range of experimentally measured tensile strengths of graywacke samples (e.g., Kubota et al., 2008; Gong and Zhao, 2014; Lu et al., 2017; Lan et al., 2019). By using the equation

$\tau = 0.5C/M$, we obtained a shear flow strength (τ) of approximately 1 MPa (with M = 6.17). At a depth of 3 km, which corresponds to a confining pressure of 80 MPa, this value is significantly lower than the friction strength (32 MPa) estimated from Byerlee's law (with a friction coefficient $\mu = 0.4$, Kohli and Zoback, 2013). Therefore, the τ value in Eqs. (13–14) should be equal to the shear flow strength of the matrix layer rather than the friction strength of the interface between the fracturing bed and the matrix layer.

In the study area, the mean ratio of vein spacing to bed thickness (s/t) for individual graywacke beds varies from 0.42 to 4.0 with a mean of 1.26 (stand deviation: 0.70) and a median of 1.02 (Fig. 11d). The s/t ratio of veins reveals a general non-linear variation with varying the bed thickness: $s/t = 3.81\ t^{-0.40}$ ($R^2 = 0.68$). When $t \geq 28.3$ cm, $s/t \leq 1$. The ratio of bed thickness to fracture spacing (t/s) for each individual bed was defined as Fracture Spacing Ratio (FSR, Gross, 1993; Bai and Pollard, 2000). Thus,

$$FSR = t/s = (\beta + t)/\alpha \tag{21}$$

FSR decreases linearly with reducing bed thickness at a rate $1/\alpha$ (Chemenda et al., 2021; Chemenda, 2022). Thus, the FSR cannot be a reliable indicator for the degree of fracture saturation over extension strain because it varies with bed thickness.

5.3. Depth of vein emplacements

The depth at which the veins formed is uncertain. The calcite and quartz in the veins have not undergone dynamic recrystallization, which suggests that the deformation temperature was relatively low and insufficient for dislocation creep and subsequent dynamic recrystallization to occur (neograins and serrated grain boundaries, Ji and Mainprice, 1990; Passchier and Trouw, 2005; Vernon, 2018) in the calcite veins (<150 °C, Kennedy and White, 2001). In contrast, vein materials from metamorphic rocks have typically undergone recrystallization (Stowell et al., 1999; Simpson, 2000). For example, quartz veins were precipitated at ~400 °C and 400 MPa in the Mona Complex metasedimentary rocks in Holy Island (Angesey, North Wales; Stowell et al., 1999).

Chi and Lavoie (1998) studied fluid inclusions trapped in fracture-filling materials in samples collected from the Rivière Ouelle and Kamouraska Formations in the Quebec Humber zone. Their microthermometric analyses revealed that the homogenization temperatures (T_h) for fluid inclusions in calcite cements range from 63 to 133 °C. These homogeneous temperatures can be taken, to a first approximation, as the temperatures at which the tensile fractures and mineralization occurred in the calcareous graywacke beds. Assuming a geothermal gradient of 30 °C/km, the burial depths are estimated to be 2.1–4.4 km at the time of calcite vein formation. Therefore, the burial depth of carbonate vein emplacements can be roughly assumed to be approximately 3 ± 1 km. The temperature estimates for calcite cementation (Chi and Lavoie, 1998) are generally consistent with those obtained using the oxygen isotope thermometer (70–92 °C) for carbonate veins in oceanic sedimentary rocks (Brandstätter et al., 2018). Additionally, the fluid inclusions measured by Chi and Lavoie (1998) have salinities of 0.9–1.7 in calcite cements, suggesting that the fluids forming the veins were most likely of local origin, such as being injected from water sills within the sedimentary basin (Vermilye and Scholz, 1995; Philipp, 2012).

As the veins were vertical when the beds were flat-lying, it can be inferred that the tensile fractures, which are perpendicular to the horizontal minimum principal stress (σ_3), formed due to an extensional regime with the maximum principal stress (σ_1) aligned vertically. Opening-mode fractures, which are characterized by the absence of shear fractures, develop only when the difference between σ_1 and σ_3 is less than or equal to 4C, where C is the tensile fracture strength (Etheridge, 1983). Using this relationship, we can estimate the maximum depths (z) at which opening-mode fractures may form in a sedimentary basin with the following equation:

$$z \leq \frac{4C(1-\nu)}{(1-2\nu)(1-\lambda)\rho g} \tag{22}$$

where C is the tensile strength of the rock, ν is the Poisson's ratio, λ is called the pore fluid factor that is the ratio of fluid pressure to lithostatic pressure, ρ is the density, and g is the gravitational acceleration. Using the values of C = 9.3 MPa, $\nu = 0.25$, $\rho = 2722$ kg/m^3, and g = 9.8 ms^{-2}, we have calculated how the depth (z) varies with changing λ. At the hydrostatic pressure ($\lambda = 1000/2722 = 0.37$), z = 3.32 km. The Gaspésie veins should form at depths smaller than 3.32 km if the pore pressure remains nearly hydrostatic in sedimentary basins. The limiting depth (z) for the fracture formation increases non-linearly with increasing λ and is 4.18 km, 5.23 km, and 6.97 km when $\lambda = 0.5$, 0.6, and 0.7, respectively. Under hydrostatic conditions, the formation temperatures of the carbonate veins, as determined by fluid inclusion thermometers (63–133 °C, Chi and Lavoie, 1998), yield a geothermal gradient varying from 19 °C/km to 40 °C/km.

5.4. Single array of veins versus orthogonal joints

The veins in the examined strata form a regular, linear arrangement with a unique orientation (Fig. 3). No cross veins are present between the systematic veins. In contrast, sedimentary strata lacking veins often exhibit orthogonal joints, which terminate against the persistent systematic joints, forming a ladder-shaped system of barren joints (Hancock, 1985; Gross, 1993; Bai et al., 2002). Such features have been documented in several regions of Quebec, Canada, including St-Jean-Port-Joli (Ji et al., 1998), Ste-Anne-des-Monts (Ji et al., 2021), Anticosti Island (Pinet et al., 2015) and Havre St-Pierre (Ji et al., 2023). The mechanical implications of the differences in geometry between the joints and veins warrant further exploration.

Following the formation of a systematic joint in a brittle layer, the local least principal stress (σ_3) is temporarily relieved in the fracture plane and the adjacent "stress shadow" regions, which prevents the initiation and propagation of fractures in the surrounding areas (Pollard and Segall, 1987). This is due to the fact that the opening mode fracture forms a free surface on which either tensile or shear stress approaches zero. As a result, a local swap between the σ_2 and σ_3 directions occurs along the joint walls and within the "stress shadows", as the effective magnitudes of these stresses are inverted, even though the remote stress field remains unchanged (Bai et al., 2002). Cross joints may then begin to form, perpendicular to the existing systematic joints, from stress-concentrated flaws or heterogeneities present in the systematic fracture walls or mechanically weak locations within the "stress shadows" (Rives et al., 1994; Boersma et al., 2018). This leads to the development of orthogonal joints through a repeating process (Ji et al., 2023). However, if the existing crack is sealed by mineral precipitation, such as in the formation of a vein, the local strength can be restored, inhibiting the permutation of stress axes (Simón, 2019), and preventing the formation of orthogonal vein networks. This is a plausible explanation for why no orthogonal vein networks occur in the Quebec Humber zone, while orthogonal barren joints are common in the regions of St-Jean-Port-Joli, Ste-Anne-des-Monts, Anticosti Island and Havre St-Pierre.

6. Conclusions

Our study has yielded the following main conclusions:

1. Veins in the Quebec Humber zone are parallel arrays of planar fractures primarily filled with carbonates. These veins are stratabound, terminating either at bedding boundaries or within the interior of the host beds. Both field evidence and numerical modeling results indicate that fracture initiation occurs at lithological interfaces or within the brittle layer's interior. Mineral precipitation

takes place when layer-parallel extension induces crack opening. The mineral deposition occurs either simultaneously or briefly after the fracture opens, as otherwise, the spacing of veins and joints would exhibit similar relationships with bed thickness. No transverse veins form perpendicular connections between the systematic veins, creating ladder-shaped orthogonal vein networks. The strength recovery resulting from sealing impedes the permutation of stress axes, thereby preventing the formation of orthogonal veins.

2. The extension strains accommodated by crack-seal processes in the graywacke beds of the Quebec Humber zone range from 1.4% to 8.5%, with a mean value of 3.8%. The veins range in width from 1 mm to 91 mm, with a median width of 7.0 mm. Vein thickness generally increases linearly with bed thickness or extension strain.
3. Both field measurements and numerical modeling data show that veins are more closely spaced than barren joints. Comparing the power-law correlation between fracture spacing and bed thickness for veins and joints provides a new method to estimate the coefficient of strength recovery (δ) through mineral precipitation for natural rocks that have undergone deformation in the past. The δ value for the carbonate veins in graywacke beds from the Quebec Humber zone is approximately 0.60, indicating that strength has been recovered by about 60% through calcite precipitation primarily due to compositional differences between the cement and host rock. This implies that efficient transfer of tensile stresses can occur across calcite veins in calcareous graywacke due to calcite cementation, but cannot occur across barren joints.
4. The burial depth of carbonate vein emplacements is estimated to be about 3 km, equivalent to a lithostatic pressure of 80 MPa. The tensile fracture strength of the graywacke and the shear flow stress of the shale during vein formation are estimated to be 9 MPa and ~ 1 MPa, respectively. The latter is much smaller than the value depicted by the friction strength of the interface between the fracturing bed and the matrix layer.

Supplementary data to this article can be found online at https://doi.org/10.1016/j.tecto.2023.230084.

CRediT authorship contribution statement

Shaocheng Ji: Writing – review & editing, Writing – original draft, Visualization, Validation, Supervision, Resources, Project administration, Methodology, Investigation, Funding acquisition, Formal analysis, Data curation, Conceptualization. **Tiantian Chen:** Visualization, Methodology, Investigation, Data curation, Conceptualization. **Le Li:** Visualization, Investigation, Data curation. **Chun'an Tang:** Validation, Supervision, Software, Project administration, Funding acquisition, Conceptualization. **Denis Marcotte:** Software, Investigation, Formal analysis.

Declaration of Competing Interest

The authors declare that they have no known competing financial interests or personal relationships that could have appeared to influence the work reported in this paper.

Data availability

Data will be made available on request.

Acknowledgments

We would like to express our gratitude for the support received from the Natural Sciences and Engineering Research Council of Canada through a discovery grant (Grant No. 06408). Furthermore, we extend our appreciation to Dr. John Hooker for his insightful discussions and to Yvéric Rousseau for drawing Fig. 1. Additionally, the authors would like to acknowledge the invaluable critical comments and helpful suggestions provided by Dr. Samuel Angiboust and the three anonymous reviewers.

References

Aben, F.M., Doan, M.L., Gratier, J.P., Renard, F., 2017. Experimental postseismic recovery of fractured rocks assisted by calcite sealing. Geophys. Res. Lett. 44 (14), 7228–7238.
Angelier, J., Souffache, B., Barrier, E., Bergerat, F., Bouaziz, S., Bouroz, C., Creuzot, G., Ouali, J., Tricart, P., 1989. Distribution de joints de tension dans un banc rocheux: loi théorique et espacements. C R Acad. Sci. Ser. 2 (309), 2119–2125.
Askeland, D.R., Fulay, P.P., Wright, W.J., 2010. The Science and Engineering of Materials, sixth ed. Cengage Learning Inc., Boston.
Bai, T., Pollard, D.D., 2000. Fracture spacing in layered rocks: a new explanation based on the stress transition. J. Struct. Geol. 22, 43–57.
Bai, T., Maerten, L., Gross, M.R., Aydin, A., 2002. Orthogonal cross joints: do they imply a regional stress rotation? J. Struct. Geol. 24, 77–88.
Bažant, Z.P., 2000. Size effect. Int. J. Solids Struct. 37 (1–2), 69–80.
Bennion, D.B., Thomas, F.B., Bietz, R.F., 1996, April. Low permeability gas reservoirs: problems, opportunities and solutions for drilling, completion, stimulation and production. In SPE gas technology symposium. OnePetro. https://doi.org/10.2118/35577-MS.
Boersma, Q., Hardebol, N., Barnhoorn, A., Bertotti, G., 2018. Mechanical factors controlling the development of orthogonal and nested fracture network geometries. Rock Mech. Rock. Eng. 51, 3455–3469.
Bowyer, M.O., Kelly, P.G., 1995. Strain and scaling relationships of faults and veins at Kilve. Somerset. Proc. USSHER Soc. 8, 411–411.
Brandstätter, J., Kurz, W., Richoz, S., Cooper, M.J., Teagle, D.A., 2018. The origin of carbonate veins within the sedimentary cover and igneous rocks of the Cocos Ridge: results from IODP Hole U1414A. Geochem. Geophys. Geosyst. 19 (10), 3721–3738.
Brooks Clark, M., Brantley, S.L., Fisher, D.M., 1995. Power-law vein-thickness distributions and positive feedback in vein growth. Geology 23 (11), 975–978.
Carpinteri, A., Chiaia, B., 1996. Power scaling laws and dimensional transitions in solid mechanics. Chaos, Solitons Fractals 7 (9), 1343–1364.
Chang, X., Lu, J., Wang, S., Wang, S., Liu, X., 2017. Formation of cracks in layered rock considering layer thickness variations. Geophys. J. Int. 210 (3), 1623–1640.
Chemenda, A.I., 2022. Bed thickness-dependent fracturing and inter-bed coupling define the nonlinear fracture spacing-bed thickness relationship in layered rocks: Numerical modeling. J. Struct. Geol. 165, 104741.
Chemenda, A.I., Lamarche, J., Matonti, C., Bazalgette, L., Richard, P., 2021. Origin of strong nonlinear dependence of fracture (joint) spacing on bed thickness in layered rocks: mechanical analysis and modeling. J. Geophys. Res. Solid Earth 126. https://doi.org/10.1029/2020JB020656 e2020JB020656.
Chen, T.T., Foulger, G.R., Tang, C.A., Mathias, S.A., Gong, B., 2022. Numerical investigation on origin and evolution of polygonal cracks on rock surfaces. Eng. Geol. 311, 106913 https://doi.org/10.1016/j.enggeo.2022.106913.
Chi, G., Lavoie, D., 1998. Porosity evolution and evidence of hydrocarbon migration in the Kamouraska and Rivière-Ouelle formations, Humber Zone, Quebec–a fluid-inclusion approach. Curr. Ther. Res. 19–24.
Clyne, T.W., Withers, P.J., 1993. An Introduction to Metal Matrix Composites. Cambridge University Press, Cambridge, UK.
Cooke, M.L., Underwood, C.A., 2001. Fracture termination and step-over at bedding interfaces due to frictional slip and interface opening. J. Struct. Geol. 23, 223–238.
Cooke, M.L., Simo, J.A., Underwood, C.A., Rijken, P., 2006. Mechanical stratigraphic controls on fracture patterns within carbonates and implications for groundwater flow. Sediment. Geol. 184 (3–4), 225–239.
Cousineau, P.A., 1998. Large-scale liquefaction and fluidization in the Cap Chat Mélange, Quebec Appalachians. Can. J. Earth Sci. 35 (12), 1408–1422. https://doi.org/10.1139/e98-076.
De Joussineau, G., Petit, J.P., 2021. Mechanical insights into the development of fracture corridors in layered rocks. J. Struct. Geol. 144, 104278.
Dobson, P.F., Kneafsey, T.J., Sonnenthal, E.L., Spycher, N., Apps, J.A., 2003. Experimental and numerical simulation of dissolution and precipitation: implications for fracture sealing at Yucca Mountain, Nevada. J. Contam. Hydrol. 62, 459–476.
Engelder, T., Fischer, M.P., 1996. Loading configurations and driving mechanisms for joints based on the Griffith energy-balance concept. Tectonophysics 256 (1–4), 253–277.
Enos, P., 1969. Cloridorme Formation, Middle Ordovician Flysch: Northern Gaspé Peninsula, Quebec, vol. 117. The Geological Society of America Inc., Boulder, Colorado.
Etheridge, M.A., 1983. Differential stress magnitudes during regional deformation and metamorphism: upper bound imposed by tensile fracturing. Geology 11, 231–234.
Fagereng, Å., 2011. Fractal vein distributions within a fault-fracture mesh in an exhumed accretionary mélange, Chrystalls Beach complex, New Zealand. J. Struct. Geol. 33 (5), 918–927.
Fischer, M.P., Gross, M.R., Engelder, T., Greenfield, R.J., 1995. Finite-element analysis of the stress distribution around a pressurized crack in a layered elastic medium: implications for the spacing of fluid-driven joints in bedded sedimentary rock. Tectonophysics 247 (1), 49–64. https://doi.org/10.1016/0040-1951(94)00200-S.
Fischer, M.P., Polansky, A., 2006. Influence of flaws on joint spacing and saturation: Results of one-dimensional mechanical modeling. J. Geophys. Res. Solid Earth 111, B07403.

Gale, J.F., Holder, J., 2010. Natural fractures in some US shales and their importance for gas production. In: Geological Society, London, Petroleum Geology Conference Series, 7. Geological Society of London, London, pp. 1131–1140. No. 1.
Gillespie, P.A., Johnston, J.D., Loriga, M.A., McCaffrey, K.J.W., Walsh, J.J., Watterson, J., 1999. Influence of layering on vein systematics in line samples. Geol. Soc. Spec. Publ. 155, 35–56.
Gillespie, P.A., Walsh, J.J., Watterson, J., Bonson, C.G., Manzocchi, T., 2001. Scaling relationships of joint and vein arrays from the Burren, Co. Clare, Ireland. J. Struct. Geol. 23 (2–3), 183–201.
Gong, F.Q., Zhao, G.F., 2014. Dynamic indirect tensile strength of sandstone under different loading rates. Rock Mech. Rock. Eng. 47, 2271–2278.
Gong, B., Wang, Y.Y., Zhao, T., Tang, C.A., Yang, X.Y., Chen, T.T., 2022. AE energy evolution during CJB fracture affected by rock heterogeneity and column irregularity under lateral pressure. Geomat. Nat. Haz. Risk 13, 877–907.
Griffiths, L., Heap, M.J., Xu, T., Chen, C.F., Baud, P., 2017. The influence of pore geometry and orientation on the strength and stiffness of porous rock. J. Struct. Geol. 96, 149–160.
Gross, M.R., 1993. The origin and spacing of cross joints: examples from the Monterey Formation, Santa Barbara Coastline, California. J. Struct. Geol. 15, 737–751.
Gross, M.R., Engelder, T., 1995. Strain accommodated by brittle failure in adjacent units of the Monterey Formation, USA: scale effects and evidence for uniform displacement boundary conditions. J. Struct. Geol. 17 (9), 1303–1318. https://doi.org/10.1016/0191-8141(95)00011-2.
Gross, M.R., Fischer, M.P., Engelder, T., Greenfield, R.J., 1995. Factors controlling joint spacing in interbedded sedimentary rocks: integrating numerical models with field observations from the Monterey Formation, USA. Geol. Soc. Spec. Publ. 92, 215–233.
Gudmundsson, A., 1999. Fluid overpressure and stress drop in fault zones. Geophys. Res. Lett. 26 (1), 115–118.
Gudmundsson, A., 2022. The propagation paths of fluid-driven fractures in layered and faulted rocks. Geol. Mag. 1–24.
Gudmundsson, A., Brenner, S.L., 2001. How hydrofractures become arrested. Terra Nova 13 (6), 456–462.
Hancock, P.L., 1985. Brittle microtectonics: principles and practice. J. Struct. Geol. 7, 437–457.
Heap, M.J., Xu, T., Chen, C.F., 2014. The influence of porosity and vesicle size on the brittle strength of volcanic rocks and magma. Bull. Volcanol. 76, 1–15.
Hesse, R., Fong, C., 2014. Umbrella structure and channel-wall stoping in the Cambrian St. Roch Formation, Quebec Appalachians: significance for particle support mechanisms and turbulence development in hyper-concentrated sediment gravity flows. Int. J. Earth Sci. 103 (2), 509–518.
Hiscott, R.N., 1978. Provenance of Ordovician deep-water sandstones, Tourelle Formation, Quebec, and implications for initiation of the Taconic orogeny. Can. J. Earth Sci. 15 (10), 1579–1597.
Hiscott, R.N., 1980. Depositional framework of sandy mid-fan complexes of Tourelle Formation, Ordovician, Quebec. AAPG Bull. 64 (7), 1052–1077. https://doi.org/10.1306/2F91942C-16CE-11D7-8645000102C1865D.
Hobbs, D.W., 1967. The formation of tension joints in sedimentary rocks: an explanation. Geol. Mag. 104, 550–556.
Hooker, J.N., Katz, R.F., 2015. Vein spacing in extending, layered rock: the effect of synkinematic cementation. Am. J. Sci. 315 (6), 557–588. https://doi.org/10.2475/06.2015.03.
Hooker, J.N., Laubach, S.E., Marrett, R., 2014. A universal power-law scaling exponent for fracture apertures in sandstones. Geol. Soc. Am. Bull. 126 (9–10), 1340–1362.
Hooker, J.N., Huggett, J.M., Cartwright, J., Ali Hussein, M., 2017. Regional-scale development of opening-mode calcite veins due to silica diagenesis. Geochem. Geophys. Geosyst. 18 (7), 2580–2600.
Hooker, J.N., Laubach, S.E., Marrett, R., 2018. Microfracture spacing distributions and the evolution of fracture patterns in sandstones. J. Struct. Geol. 108, 66–79.
Ji, S., 2022. Relationship between fracture spacing and bed thickness in sedimentary rocks: Approach by means of Michaelis–Menten equation. J. Rock Mech. Geotech. Eng. https://doi.org/10.1016/j.jrmge.2022.11.003.
Ji, S., Li, L., 2020. An alternative interpretation for the formation of doubly plunging folds in sandstone terrains. Terra Nova 32 (5), 325–333. https://doi.org/10.1111/ter.12469.
Ji, S., Mainprice, D., 1990. Recrystallization and fabric development in plagioclase. J. Geol. 98 (1), 65–79.
Ji, S., Saruwatari, K., 1998. A revised model for the relationship between joint spacing and layer thickness. J. Struct. Geol. 20 (11), 1495–1508.
Ji, S., Zhu, Z., Wang, Z., 1998. Relationship between joint spacing and bed thickness in sedimentary rocks: effects of interbed slip. Geol. Mag. 135 (5), 637–655.
Ji, S., Li, L., Marcotte, D., 2021. Power-law relationship between joint spacing and bed thickness in sedimentary rocks and implications for layered rock mechanics. J. Struct. Geol., 104413 https://doi.org/10.1016/j.jsg.2021.104413.
Ji, S., Rousseau, Y., Marcotte, D., Phillips, N.J., 2023. The formation of orthogonal joint systems and cuboidal blocks: New insights gained from flat-lying limestone beds in the region of Havre-Saint-Pierre (Quebec, Canada). J. Rock Mech. Geotech. Eng. https://doi.org/10.1016/j.jrmge.2023.03.012.
Jones, T.A., Detwiler, R.L., 2016. Fracture sealing by mineral precipitation: the role of small-scale mineral heterogeneity. Geophys. Res. Lett. 43 (14), 7564–7571.
Kennedy, L.A., White, J.C., 2001. Low-temperature recrystallization in calcite: Mechanisms and consequences. Geology 29 (11), 1027–1030.
Kohli, A.H., Zoback, M.D., 2013. Frictional properties of shale reservoir rocks. J. Geophys. Res. Solid Earth 118 (9), 5109–5125.
Korach, C.S., Keer, L.M., 2002. Stresses between 3D fractures in infinite and layered elastic solids. Eng. Fract. Mech. 69 (17), 1815–1825.
Kubota, S., Ogata, Y., Wada, Y., Simangunsong, G., Shimada, H., Matsui, K., 2008. Estimation of dynamic tensile strength of sandstone. Int. J. Rock Mech. Min. Sci. 45 (3), 397–406.
Lan, H., Chen, J., Macciotta, R., 2019. Universal confined tensile strength of intact rock. Sci. Rep. 9, 1–9.
Lavoie, D., 2008. Appalachian foreland basin of Canada. In: Hsu, K.J. (Ed.), Sedimentary Basins of the World Series: The Sedimentary Basin of the USA and Canada. Elsevier, Amsterdam, pp. 63–103.
Lavoie, D., Burden, E., Lebel, D., 2003. Stratigraphic framework for the Cambrian Ordovician rift and passive margin successions from southern Quebec to western Newfoundland. Can. J. Earth Sci. 40 (2), 177–205.
Lavoie, D., Pinet, N., Dietrich, J., Hannigan, P., Castonguay, S., Hamblin, A.P., Giles, P., 2009. Petroleum resource assessment, Paleozoic successions of the St. Lawrence Platform and Appalachians of eastern Canada. In: Geological Survey of Canada, Open File, 6174.
Lawn, B., 1995. Fracture of Brittle Solids, second ed. Cambridge University Press, Cambridge, UK.
Lee, Y.J., Morse, J.W., 1999. Calcite precipitation in synthetic veins: implications for the time and fluid volume necessary for vein filling. Chem. Geol. 156 (1–4), 151–170. https://doi.org/10.1016/S0009-2541(98)00183-1.
Lee, H.P., Olson, J.E., Holder, J., Gale, J.F., Myers, R.D., 2015. The interaction of propagating opening mode fractures with pre-existing discontinuities in shale. J. Geophys. Res. Solid Earth 120 (1), 169–181.
Levi, T., Avni, Y., Bahat, D., 2019. Evolution of the stress field near the Arava basin located along the Dead Sea Fault system as revealed by joint sets. J. Struct. Geol. 128, 103876.
Li, L., Ji, S., 2021. A new interpretation for formation of orthogonal joints in quartz sandstone. J. Rock Mech. Geotech. Eng. 13 (2), 289–299. https://doi.org/10.1016/j.jrmge.2020.08.003.
Li, Y., Yang, C., 2007. On fracture saturation in layered rocks. Int. J. Rock Mech. Min. Sci. 44, 936–941.
Lloyd, G.E., Ferguson, C.C., Reading, K., 1982. A stress-transfer model for the development of extension fracture boudinage. J. Struct. Geol. 4 (3), 355–372. https://doi.org/10.1016/0191-8141(82)90019-0.
Lobo-Guerrero, S., Vallejo, L.E., 2006. Application of Weibull statistics to the tensile strength of rock aggregates. J. Geotech. Geoenviron. Eng. 132 (6), 786–790.
Lu, C., Sun, Q., Zhang, W., Geng, J., Qi, Y., Lu, L., 2017. The effect of high temperature on tensile strength of sandstone. Appl. Therm. Eng. 111, 573–579.
Lynch, G., 1998. Characteristics of the Taconic orogenic front, Northeastern Québec Appalachians. Curr. Ther. Res. 1–9.
Lynch, G., Arsenault, O., 1997. Stratigraphy and deformation of the Humber zone in Gaspésie Québec. Curr. Ther. Res. 1–8.
Malhame, P., Hesse, R., 2015. Quartz arenites of the Cambro–Ordovician Kamouraska Formation, Quebec Appalachians, Canada: II. Eolian sands in deep-sea sedimentary gravity-flow deposits. Can. J. Earth Sci. 52 (4), 261–277. https://doi.org/10.1139/cjes-2014-0030.
Malo, M., 2004. Paleogeography of the Matapédia basin in the Gaspé Appalachians: initiation of the Gaspé Belt successor basin. Can. J. Earth Sci. 41 (5), 553–570. https://doi.org/10.1139/e03-100.
Malo, M., Tremblay, A., Kirkwood, D., Cousineau, P., 1995. Along-strike Acadian structural variations in the Québec Appalachians: consequence of a collision along an irregular margin. Tectonics 14 (6), 1327–1338.
Marrett, R., Gale, J.F., Gómez, L.A., Laubach, S.E., 2018. Correlation analysis of fracture arrangement in space. J. Struct. Geol. 108, 16–33.
Masuda, T., Kuriyama, M., 1988. Successive “mid-point” fracturing during microboudinage: an estimate of the stress-strain relation during a natural deformation. Tectonophysics 147, 171–177.
Michaelis, L., Menten, M.L., 1913. Die Kinetik der Invertinwirkung. Biochem. Z. 49, 333–369.
Morrison, J.K., Shah, S.P., Jenq, Y.S., 1988. Analysis of fiber debonding and pullout in composites. J. Eng. Mech. 114, 277–294.
Morrow, C.A., Moore, D.E., Lockner, D.A., 2001. Permeability reduction in granite under hydrothermal conditions. J. Geophys. Res. Solid Earth 106 (B12), 30551–30560. https://doi.org/10.1029/2000JB000010.
Narr, W., Suppe, J., 1991. Joint spacing in sedimentary rocks. J. Struct. Geol. 13 (9), 1037–1048. https://doi.org/10.1016/0191-8141(91)90055-N.
Olivier, G., Brenguier, F., Campillo, M., Roux, P., Shapiro, N.M., Lynch, R., 2015. Investigation of coseismic and postseismic processes using in situ measurements of seismic velocity variations in an underground mine. Geophys. Res. Lett. 42 (21), 9261–9269. https://doi.org/10.1002/2015GL065975.
Olson, J., Pollard, D.D., 1989. Inferring paleostresses from natural fracture patterns: a new method. Geology 17 (4), 345–348.
Pakzad, R., Wang, S.Y., Sloan, S., 2018. Numerical study of the failure response and fracture propagation for rock specimens with preexisting flaws under compression. Int. J. Geomech. 18 (7), 04018070.
Parkash, B., 1970. Downcurrent changes in sedimentary structures in Ordovician turbidite greywackes. J. Sediment. Res. 40 (2), 572–590.
Passchier, C.W., Trouw, R.A., 2005. Microtectonics. Springer Science & Business Media, Berlin, Germany.
Paterson, M.S., Wong, T.F., 2005. Experimental Rock Deformation-the Brittle Field. Springer Science & Business Media, Berlin, Germany.
Peacock, D.C.P., 2004. Differences between veins and joints using the example of the Jurassic limestones of Somerset. Geol. Soc. Spec. Publ. 231 (1), 209–221. https://doi.org/10.1144/GSL.SP.2004.231.01.12.
Philipp, S.L., 2008. Geometry and formation of gypsum veins in mudstones at Watchet, Somerset, SW England. Geol. Mag. 145 (6), 831–844.

Philipp, S.L., 2012. Fluid overpressure estimates from the aspect ratios of mineral veins. Tectonophysics 581, 35–47.
Pincivy, A., 2003. Géochronologie $^{40}Ar/^{39}Ar$ et analyse structurale de la zone de Humber des Appalaches de Gaspésie (Québec, Canada): implication sur la tectonique des Appalaches du nord. Université du Québec, Québec. Doctoral dissertation.
Pinet, N., Lavoie, D., Keating, P., Duchesne, M., 2014. The St Lawrence Platform and Appalachian deformation front in the St Lawrence Estuary and adjacent areas (Quebec, Canada): structural complexity revealed by magnetic and seismic imaging. Geol. Mag. 151, 996–1012.
Pinet, N., Brake, V., Lavoie, D., 2015. Geometry and regional significance of joint sets in the Ordovician-Silurian Anticosti Basin: new insights from fracture mapping. In: Geological Survey of Canada, Open File, 7752, p. 24.
Pollard, D.D., Segall, P., 1987. Theoretical displacements and stresses near fractures in rock: With applications to faults, joints, veins, dikes, and solution surfaces. In: Atkinson, A.K. (Ed.), Fracture Mechanics of Rock. Elsevier, Amsterdam, Netherlands, pp. 277–347.
Price, N.J., Cosgrove, J.W., 1990. Analysis of Geological Structures. Cambridge University Press, Cambridge, UK.
Ramsay, J.G., 1980. The crack-seal mechanism of rock deformation. Nature 284 (5752), 135–139. https://doi.org/10.1038/284135a0.
Rives, T., Rawnsley, K.D., Petit, J.P., 1994. Analogue simulation of natural orthogonal joint set formation in brittle varnish. J. Struct. Geol. 16, 419–429.
Rustichelli, A., Tondi, E., Agosta, F., Di Celma, C., Giorgioni, M., 2013. Sedimentologic and diagenetic controls on pore-network characteristics of Oligocene–Miocene ramp carbonates (Majella Mountain, central Italy) Sedimentologic and Diagenetic Controls on Pore-Network Characteristics. AAPG Bull. 97 (3), 487–524.
Scholz, C.H., Cowie, P.A., 1990. Determination of total strain from faulting using slip measurements. Nature 346 (6287), 837–839.
Schöpfer, M.P., Arslan, A., Walsh, J.J., Childs, C., 2011. Reconciliation of contrasting theories for fracture spacing in layered rocks. J. Struct. Geol. 33, 551–565.
Shang, J., Hencher, S.R., West, L.J., 2016. Tensile strength of geological discontinuities including incipient bedding, rock joints and mineral veins. Rock Mech. Rock. Eng. 49, 4213–4225.
Sibson, R.H., Robert, F., Poulsen, K.H., 1988. High-angle reverse faults, fluid-pressure cycling, and mesothermal gold-quartz deposits. Geology 16 (6), 551–555.
Simón, J.L., 2019. Forty years of paleostress analysis: has it attained maturity? J. Struct. Geol. 125, 124–133.
Simpson, G.D.H., 2000. Synmetamorphic vein spacing distributions: characterisation and origin of a distribution of veins from NW Sardinia, Italy. J. Struct. Geol. 22 (3), 335–348.
Skipper, K., Middleton, G.V., 1975. The sedimentary structures and depositional mechanics of certain Ordovician turbidites, Cloridorme Formation, Gaspé Peninsula, Québec. Can. J. Earth Sci. 12 (11), 1934–1952.
Slivitzky, A., St-Julien, P., Lachambre, G., 1991. Synthèse géologique du Cambro-Ordovicien du nord de la Gaspésie. In: Ministère de l'Énergie et des Ressources du Québec, pp. ET88–14.
Souffaché, B., Angelier, J., 1989. Distribution de joints de tension dans un banc rocheux: principe d'une modélisation énergétique. C R Acad. Sci. Ser. 2308 (15), 1385–1390.
Späth, M., Urai, J.L., Nestler, B., 2022. Incomplete crack sealing causes localization of fracturing in hydrothermal quartz veins. Geophys. Res. Lett. 49 (15) e2022GL098643.
St-Julien, P., 1967. Tectonics of part of the appalachian region of southeastern Quebec (southwest of the Chaudière River). In: Appalachian Tectonics. University of Toronto Press, Toronto, pp. 41–47.
St-Julien, P., Hubert, C., 1975. Evolution of the Taconian orogen in the Quebec Appalachians. Am. J. Sci. 275, 337–362.
St-Julien, P., Slivitzky, A., Feininger, T., Hatcher Jr., R.D., 1983. A deep structural profile across the Appalachians of southern Québec. In: Williams, H., Zeitz, I. (Eds.), Contributions to the Tectonics and Geophysics of Mountain Chains. Geological Society of America, pp. 103–111.
Stowell, J.F., Watson, A.P., Hudson, N.F., 1999. Geometry and population systematics of a quartz vein set, Holy Island, Anglesey, North Wales. Geol. Soc. Spec. Publ. 155 (1), 17–33.
Strong, P.G., Walker, R.G., 1981. Deposition of the Cambrian continental rise: the St. Roch Formation near St. Jean-Port-Joli, Quebec. Can. J. Earth Sci. 18, 1320–1335.
Tang, C., 1997. Numerical simulation of progressive rock failure and associated seismicity. Int. J. Rock Mech. Min. Sci. 34, 249–261.
Tang, C.A., Zhang, Y.B., Liang, Z.Z., Xu, T., Tham, L.G., Lindqvist, P.A., Kou, S.Q., Liu, H. Y., 2006. Fracture spacing in layered materials and pattern transition from parallel to polygonal fractures. Phys. Rev. E 73, 056120.
Tang, C.A., Liang, Z.Z., Zhang, Y.B., 2008. Fracture spacing in layered materials: a new explanation based on two-dimensional failure process modelling. Am. J. Sci. 308, 49–72.
Tang, C.A., Webb, A.A.G., Moore, W.B., Wang, Y.Y., Ma, T.H., Chen, T.T., 2020. Breaking Earth's shell into a global plate network. Nat. Commun. 11 (1), 1–6.
Tenthorey, E., Cox, S.F., 2006. Cohesive strengthening of fault zones during the interseismic period: an experimental study. J. Geophys. Res. Solid Earth 111 (B9). https://doi.org/10.1029/2005JB004122.
Tenthorey, E., Cox, S.F., Todd, H.F., 2003. Evolution of strength recovery and permeability during fluid-rock reaction in experimental fault zones. Earth Planet. Sci. Lett. 206 (1–2), 161–172.
Tinni, A., Sondergeld, C., Chandra, R., 2019. Hydraulic fracture propagation velocity and implications for hydraulic fracture diagnostics. In: 53rd US Rock Mechanics/ Geomechanics Symposium. American Rock Mechanics Association.
Tobler, D.J., Minto, J.M., El Mountassir, G., Lunn, R.J., Phoenix, V.R., 2018. Microscale analysis of fractured rock sealed with microbially induced $CaCO_3$ precipitation: influence on hydraulic and mechanical performance. Water Resour. Res. 54 (10), 8295–8308.
Tripathi, D., Jones, F.R., 1998. Single fibre fragmentation test for assessing adhesion in fibre reinforced composites. J. Mater. Sci. 33, 1–16.
Van Noten, K., Sintubin, M., 2010. Linear to non-linear relationship between vein spacing and layer thickness in centimetre-to decimetre-scale siliciclastic multilayers from the High-Ardenne slate belt (Belgium, Germany). J. Struct. Geol. 32 (3), 377–391.
Vass, A., Koehn, D., Toussaint, R., Ghani, I., Piazolo, S., 2014. The importance of fracture-healing on the deformation of fluid-filled layered systems. J. Struct. Geol. 67, 94–106.
Vermilye, J.M., Scholz, C.H., 1995. Relation between vein length and aperture. J. Struct. Geol. 17 (3), 423–434.
Vernon, R.H., 2018. A practical guide to rock microstructure. Cambridge University Press.
Virgo, S., Abe, S., Urai, J.L., 2014. The evolution of crack seal vein and fracture networks in an evolving stress field: insights from discrete element models of fracture sealing. J. Geophys. Res. Solid Earth 119 (12), 8708–8727.
Wang, Q., Chen, X., Jha, A.N., Rogers, H., 2014. Natural gas from shale formation–the evolution, evidences and challenges of shale gas revolution in United States. Renew. Sust. Energ. Rev. 30, 1–28.
Wasantha, P.L.P., Ranjith, P.G., Xu, T., Zhao, J., Yan, Y.L., 2014. A new parameter to describe the persistency of non-persistent joints. Eng. Geol. 181, 71–77.
Weibull, W., 1952. A survey of statistical effects in the field of material failure. Appl. Mech. Rev. 5 (11), 449–451.
Williams, H., 1995. Geology of the Appalachian—Caledonian Orogen in Canada and Greenland. The Geological Society of America Inc., Boulder, Colorado.
Wong, T.F., Wong, R.H., Chau, K.T., Tang, C.A., 2006. Microcrack statistics, Weibull distribution and micromechanical modeling of compressive failure in rock. Mech. Mater. 38 (7), 664–681.
Yasuhara, H., Marone, C., Elsworth, D., 2005. Fault zone restrengthening and frictional healing: the role of pressure solution. J. Geophys. Res. Solid Earth 110 (B6).
Zhao, P., Ji, S., 1997. Refinements of shear-lag model and its applications. Tectonophysics 279 (1–4), 37–53.